Development/Plasticity/Repair

p63 Regulates Adult Neural Precursor and Newly Born Neuron Survival to Control Hippocampal-Dependent Behavior

Gonzalo I. Cancino,[1,2] Adelaide P. Yiu,[3]* Michael P. Fatt,[1,2,4]* Chandrasagar B. Dugani,[1,2,4] Elsa R. Flores,[7] Paul W. Frankland,[3,5] Sheena A. Josselyn,[3,5] Freda D. Miller,[2,4,5,6] and David R. Kaplan[1,4,6]

Programs in [1]Cell Biology, [2]Developmental and Stem Cell Biology, and [3]Neurosciences and Mental Health, Hospital for Sick Children, Toronto, Ontario M5G 1X8, Canada, [4]Institute of Medical Science and Departments of [5]Physiology and [6]Molecular Genetics, University of Toronto, Toronto, Ontario M5S 1A8, Canada, and [7]Department of Biochemistry and Molecular Biology, The University of Texas M.D. Anderson Cancer Center, Houston, Texas 77030

The molecular mechanisms that regulate adult neural precursor cell (NPC) survival, and thus maintain adult neurogenesis, are not well defined. Here, we investigate the role of p63, a p53 family member, in adult NPC function in mice. Conditional ablation of p63 in adult NPCs or p63 haploinsufficiency led to reduced numbers of NPCs and newborn neurons in the neurogenic zones of the hippocampus and lateral ventricles and in the olfactory bulb. These reductions were attributable to enhanced apoptosis of NPCs and newborn neurons and were rescued by inhibition of caspase activity, p53, or the p53 apoptotic effector PUMA (p53-upregulated modulator of apoptosis). Moreover, these cellular deficits were functionally important because they led to perturbations in hippocampus-dependent memory formation. These results indicate that p63 regulates the numbers of adult NPCs and adult-born neurons as well as neural stem cell-dependent cognitive functions, and that it does so, at least in part, by inhibiting p53-dependent cell death.

Introduction

In the adult mammalian central nervous system (CNS), neurogenesis is thought to generate functional neurons throughout life. Neural stem and progenitor cells reside in two neurogenic regions of the CNS, the dentate gyrus subgranular zone (SGZ) of the hippocampus and the subventricular zone (SVZ) of the lateral ventricles, in which they generate dentate granule cells and olfactory bulb interneurons, respectively (Deng et al., 2010; Ming and Song, 2011). In the rodent hippocampus, neurogenesis contributes to the formation and consolidation of several forms of hippocampal-dependent memory, whereas in the olfactory bulb, it regulates aspects of olfactory learning. A variety of extrinsic cues positively regulate adult NPC number and function, including growth factors and cytokines, exercise, pregnancy, and learning, whereas pathological events associated with aging, stress, and neurodegeneration negatively regulate neurogenesis.

Received March 22, 2013; revised May 28, 2013; accepted June 24, 2013.

Author contributions: G.I.C., F.D.M., and D.R.K. designed research; G.I.C., A.P.Y., M.P.F., and C.B.D. performed research; E.R.F. contributed unpublished reagents/analytic tools; G.I.C., A.P.Y., P.W.F., and S.A.J. analyzed data; G.I.C., P.W.F., S.A.J., F.D.M., and D.R.K. wrote the paper.

This work was funded by Canadian Institutes of Health Research Grants MOP-38021 and MOP-14446 (F.D.M., D.R.K.). G.I.C. is funded by fellowships from the Heart and Stroke Foundation of Canada and Becas Chile. F.D.M. and D.R.K. hold Canada Research Chairs, and F.D.M. is a Howard Hughes Medical Institute International Research Scholar. We thank Alea Mills (Cold Spring Harbor Laboratory) for the generous gift of the $p63^{-/-}$ and $p63^{fl/fl}$ mice. We thank Benigno Aquino and Vania Ariosa for technical assistance.

*A.P.Y. and M.P.F. contributed equally to this work.

The authors declare no competing financial interests.

Correspondence should be addressed to both David R. Kaplan and Freda Miller, The Hospital for Sick Children, 555 University Avenue, Toronto, ON, Canada M5G 1X8. E-mail: dkaplan@sickkids.ca, fredam@sickkids.ca.

DOI:10.1523/JNEUROSCI.1251-13.2013

 0270-6474/13/3312569-17$15.00/0

A precise and delicate balance between self-renewal, proliferation, survival, and differentiation is required for NPCs to contribute to cognitive function. Although much is known about the genes and signaling proteins that regulate self-renewal, proliferation, and neurogenesis, little is known about those that regulate NPC survival. In the adult SGZ and SVZ, basal and ongoing apoptosis is regulated by the apoptosome component AIF (apoptosis-inducing factor) and the BH3 (Bcl-2 homology domain 3) family proteins BIM (Bcl-2 interacting mediator of cell death), PUMA, and MCL1 (myeloid cell leukemia sequence 1) that function at the mitochondria (Bunk et al., 2010; Malone et al., 2012; Sun et al., 2012). These proteins are regulated by p53 in other cell types, and p53 deletion increases the survival of SVZ-derived neurospheres (Meletis et al., 2006). We previously implicated p63 in the survival of embryonic NPCs (Dugani et al., 2009), although there is no apparent CNS or NPC phenotype in $p63^{-/-}$ embryos (Holembowski et al., 2011). However, we did not ask about a role for p63 in adult neural precursors, which are regulated by different stimuli and have very different functions from embryonic NPCs.

The p53 family of transcription factors, which includes p53, p63, and p73, share similar transactivation, DNA binding, and oligomerization domains. p63 and p73 exist as N-terminal truncated (ΔN) and full-length (TA) isoforms attributable to alternative promoter usage, with the truncation deleting most of the transcriptional activation potential of the proteins (Dötsch et al., 2010). The truncated isoforms suppress full-length isoform activity by at least two mechanisms, by forming inactive heterodimers with full-length members, or by binding to and repressing p53 family transcriptional promoters (Dötsch et

al., 2010). The ΔN isoforms also directly suppress kinases such as JNK (Wetzel et al., 2008).

p73 plays a prominent role in regulating the self-renewal and proliferation of NPCs (Fujitani et al., 2010; Talos et al., 2010; Flores, 2011), and ΔNp73 is critical for the survival of neurons in the postnatal and adult rodent brain (Pozniak et al., 2002; Wetzel et al., 2008; Tissir et al., 2009). This led us to ask whether other ΔN isoforms mediate survival of adult neural cell types. Here, we identify ΔNp63 as a key prosurvival protein for adult NPCs and show that decreased survival of NPCs and adult-born neurons resulting from perturbation of p63 has important repercussions for cognitive function.

Materials and Methods

Animals and tamoxifen treatment. This study was approved by the Hospital for Sick Children Animal Care Committee, in accordance with Canadian Council on Animal Care guidelines. $p63^{+/-}$ mice (Mills et al., 1999) were maintained on a C57BL/6 background as described previously (Dugani et al., 2009). $p53^{-/-}$ mice (Jacks et al., 1994) were acquired from The Jackson Laboratory, crossed with $p63^{+/-}$ mice, and maintained on a C57BL/6 background. $p63^{fl/fl}$ mice (Mills et al., 2002) were crossed with $Rosa26R^{YFP/YFP}$ reporter mice (Lagace et al., 2007) and *nestin–CreERT2*$^{+/\varnothing}$ mice (Imayoshi et al., 2008) and then maintained through homozygous breeding pairs on a C57BL/6 background. $p63^{fl/fl}$ mice were maintained through homozygous breeding pairs for neurosphere assays. For behavioral studies and neuroanatomical analyses, 1- or 2-month-old $p63^{+/+}$;*nestin–CreERT2*$^{+/\varnothing}$;$Rosa26R^{YFP/YFP}$ and $p63^{fl/fl}$;*nestin–CreERT2*$^{+/\varnothing}$;$Rosa26R^{YFP/YFP}$ mice were injected intraperitoneally daily with tamoxifen (180 mg/kg in sunflower oil) for 5 consecutive days, followed by 3 weeks of rest for three rounds. Mice had access to rodent chow and water *ad libitum* in a 12 h light/dark cycle room. Animals of both sexes were used in these studies.

Neuroanatomy. For histology and immunocytochemistry, mice were killed with a sodium pentobarbital overdose and transcardially perfused with PBS, followed by 4% paraformaldehyde. $p63^{+/-}$ mice, crossed or not to $p53^{-/-}$ mice, were all analyzed neuroanatomically at 3 months of age, whereas $p63^{fl/fl}$ mice were all analyzed at 5 months of age, after tamoxifen treatment. Brains were cryoprotected and sectioned at 18 μm. Immunohistochemistry was performed as described previously (Cancino et al., 2008, 2013). Briefly, sections were washed with TBS buffer, permeabilized with TBS, 0.3% Triton X-100 solution, and then incubated in TBS, 5% BSA, 0.3% Triton X-100 for 1 h as a blocking solution. Slides were incubated with primary antibodies in blocking solution at 4°C overnight. After TBS washes, the sections were incubated with secondary antibodies in blocking solution for 1 h at room temperature. Finally, after TBS washes, sections were mounted in Permount solution (Thermo Fisher Scientific). Digital image acquisition was performed with Axiovision software (Carl Zeiss) on a Carl Zeiss Axioplan 2 microscope with a Hamamatsu Orca-R2 CCD video camera or with Volocity (PerkinElmer Life and Analytical Sciences) software on an Olympus IX81F-3 confocal microscope with a Hamamatsu EM-CCD video camera. Nissl staining was performed as described previously (Pozniak et al., 2002). For quantification of dentate gyrus thickness, the thickness of the upper and lower blades was measured at three different points in 20 sections per animal that spanned the rostrocaudal extent of the hippocampus. For immunocytochemical analysis of cell types in the hippocampal SGZ, serial coronal 18 μm sections were collected spanning the rostrocaudal extent of the hippocampus. In all cases, for quantification, every 10th section was selected for a total of 10 representative, matched sections per hippocampus. Every positive cell was counted on these sections, and, to obtain the relative total number of cells in the dentate gyrus, these counts were multiplied by 10 to account for the sampling frequency. For analysis of the SVZ, serial coronal 18 μm sections were collected spanning the rostrocaudal extent of the SVZ. For quantification, every 10th section was selected for a total of 10 representative sections per SVZ, which were matched in terms of neuroanatomical level. Every positive cell was counted on these sections in all cases. For analysis of the olfactory bulb, serial coronal 18 μm sections were collected that spanned the rostrocaudal extent of the olfactory bulb. For quantification, every 10th section was selected for a total of 10 matched representative sections per olfactory bulb. Every positive cell was counted on these sections, and, to obtain the relative total number of cells in the olfactory bulb, these counts were multiplied by 10 to account for the sampling frequency. To quantify the proportion of Sox2-positive or doublecortin (DCX)-positive cells that were also positive for cleaved caspase-3 (CC3), TUNEL, or p63 in the dentate gyrus and SVZ, 10 sections were sampled as above and immunostained, and the total numbers of cells positive for one or both markers were counted and expressed as a percentage of double-positive/single-positive cells. Ninety to 300 double-labeled cells were counted per brain, as specified in the figure legends. To quantify the proportion of NeuN-positive cortical neurons that were p63 positive, five coronal sections at the level of the hippocampus, sampled every 10th serial section, were immunostained, and one randomly selected field per section over layer III/IV of the cortex was quantified for the number of single- and double-positive cells.

For quantification of granule cell density in the dentate gyrus, serial 18-μm-thick coronal sections through the rostrocaudal extent of the hippocampus were collected, and every cell in a 2500 μm^2 area (50 × 50 μm) was counted on every 10th section. Ten different square areas were quantified per section. To obtain dentate gyrus area, the total length of the dentate gyrus, including the upper and lower blades, was measured on every 10th section, and this was multiplied by the average dentate gyrus thickness (described above). To obtain the number of granule cells in the dentate gyrus, the total dentate gyrus area was multiplied by the cell density, and then this was multiplied by 10 to account for the sampling frequency.

BrdU labeling. For quantification of the proportion of proliferating SGZ or SVZ neural precursors, a single injection of 100 mg/kg BrdU (Sigma-Aldrich) was administered intraperitoneally at 3 months of age for control and $p63^{+/-}$ mice, crossed or not to $p53^{-/-}$ mice. Twenty-four hours after administration, mice were killed by sodium pentobarbital overdose and transcardially perfused with PBS, followed by 4% paraformaldehyde. Brains were postfixed overnight, and the hippocampus or the SVZ was sectioned coronally on a cryostat at 18 μm. Ten hippocampal or SVZ sections, sampled every 10th section, were analyzed immunocytochemically for BrdU as described previously (Fujitani et al., 2010). For the SGZ, we quantified all BrdU-labeled nuclei in the SGZ (defined as two cell diameters beneath the granule cell layer). For the SVZ, we quantified all BrdU-labeled nuclei. To perform the Sox2/BrdU analysis, sections were incubated in 1N HCl at 60°C for 30 min, rinsed in PBS, incubated in rat anti-BrdU antibody at 4°C overnight, and then in Alexa Fluor 488 donkey anti-rat antibody for 2 h, followed by sequential immunostaining with anti-Sox2 and by an Alexa Fluor 555-conjugated donkey anti-mouse secondary antibody. The total numbers of Sox2-positive, BrdU-positive, and double-labeled Sox2/BrdU-positive cells were then quantified in 10 sections through the SGZ or SVZ, sampled every 10 serial sections. To quantify adult-born hippocampal or olfactory bulb neurons, mice were injected with 60 mg/kg BrdU intraperitoneally every 3 h for five injections and killed 30 d later. For the $p63^{+/-}$ mice, crossed or not to the $p53^{-/-}$ mice, animals were injected at 2 months of age and analyzed at 3 month of age, whereas for $p63^{fl/fl}$ mice, animals were injected at 4 months of age (after the second month of tamoxifen injection) and analyzed at 5 months. Animals were killed, and brains were fixed and cryoprotected as above. The hippocampi or olfactory bulbs were then cryosectioned serially at 18 μm throughout their rostrocaudal extent. Every 10th serial section was immunostained, for a total of 10 sections per brain. To perform immunostaining, sections were incubated in 1N HCl at 60°C for 30 min, rinsed in PBS, incubated in rat anti-BrdU antibody at 4°C overnight, and then in Alexa Fluor 488 donkey anti-rat antibody for 2 h, followed by sequential immunostaining with anti-NeuN and by an Alexa Fluor 555-conjugated donkey anti-mouse secondary antibody. The total numbers of BrdU/NeuN double-labeled cells in the granule cell layers were counted, and, to obtain the total number of BrdU-positive adult-born neurons, these numbers were multiplied by 10 to account for sampling frequency.

Culture experiments. For adult SVZ neurospheres, the subependyma of the lateral ventricle was dissected and dissociated as described previously

(Fujitani et al., 2010). Cell density and viability were determined using trypan blue. Cells were cultured under clonal conditions at 10 cells/μl in six-well (2 ml/well) ultra-low attachment dishes (Corning) in serum-free medium containing 20 ng/ml EGF (Sigma-Aldrich), 10 ng/ml FGF2 (Sigma-Aldrich), and 2 μg/ml heparin (Sigma-Aldrich). Cells from each animal were cultured individually, and triplicates were performed for each condition and each animal. Sphere number was counted after 6 d; only colonies of at least 10 cells were counted as spheres. To assay self-renewal, neurospheres were mechanically dissociated into single cells, passed through a cell strainer, and cultured as for primary cultures, and spheres were counted after 4 d. For acute genetic ablation of p63 and its isoforms, primary neurospheres 3 d after culture from the SVZ of $p63^{fl/fl}$, TA$p63^{fl/fl}$, and ΔN$p63^{fl/fl}$ mice were infected with 25 multiplicity of infection (M.O.I.) recombinant adenovirus (Ad5) expressing EGFP or Cre recombinase (Vector Laboratories), and total neurosphere numbers were quantified 3 d later. For ZVAD studies, cells were infected as above, 50 μM ZVAD (Z-VAD-FMK (carbobenzoxy-valyl-alanyl-aspartyl-[O-methyl]- fluoromethylketone)) was added 1 d later, and total neurosphere numbers were quantified after an additional 3 d. For the lentivirus experiments, ΔN$p63^{fl/fl}$ or $p63^{fl/fl}$ SVZ cells were cultured for 2 d, infected with 10 M.O.I. of recombinant lentivirus encoding a scrambled or previously characterized p53 shRNA (Santa Cruz Biotechnology), and then infected again 2 d later with recombinant lentivirus expressing EGFP or Cre recombinase. Total neurosphere numbers were quantified 3 d later. For tamoxifen administration *in vitro*, tamoxifen was dissolved in DMSO so that the final volume of DMSO was ~0.1% of the total volume of medium. In all experiments, DMSO alone was used as a vehicle control. Postnatal day 5 dentate gyrus neurospheres were cultured as described previously (Fujitani et al., 2010). Skin-derived precursors were isolated from the neonatal whisker pads as described previously (Biernaskie et al., 2006).

RT-PCR. RNA was extracted from samples using Trizol Reagent (Invitrogen) and was treated with DNase I (Fermentas) to remove contaminating genomic DNA. One microgram of DNase-treated RNA was then reverse transcribed using RevertAid H Minus M-MulV Reverse Transcriptase (Fermentas) with the provided oligo-dT_{18} primers. This template was subsequently used for PCR with the following primers: pan-p63 forward, 5′-GACCGGAAGGCAGATGAAGACAG-3′; pan-p63 reverse, 5′-TGTTTCTGAAGTAGGTGCTGGTGC-3′; ΔNp63 forward, 5′-GGAAAACAATGCCCAGACTC-3′; ΔNp63 reverse, 5′-GATGGAGAGAGGGCATCAAA-3′; TAp63 forward, 5′-AACCCCAGCTCATTTCTCGT-3′; TAp63 reverse, 5′-GGCCCGGGTAATCTGTGTTGG-3′; GAPDH forward, 5′-ACGGCAAGTTCAATGGCACAGTCA-3′; GAPDH reverse; 5′-GCTTTCCAGAGGGGCCATCCACAG-3′; p73 forward, 5′-CCTGTCATCCCTTCCAATACC-3′; p73 reverse, 5′-ACAACCACACTCTGCCTTC-3′; p53 forward, 5′-GCAGTCTGGGACAGCCAAG-3′; p53 reverse, 5′-GGTAAGGATAGGTCGGCGG-3′; PUMA forward, 5′-TGGGTGCACTGATGGAGATA-3′; and PUMA reverse, 5′-AACCTATGCAATGGGATGGA-3′. For p63α/β/γ, a common forward primer was used (5′-AAGAGACCGGAAGGCAGATGAAG-3′), with isoform-specific reverse primers as follows: p63α reverse, 5′-ACGGGGTGGAAAAGAGATGGTC-3′; p63β reverse, 5′-GACTTGCCAAATCCTGACA-3′; and p63γ reverse, 5′-CTCCCCGGGGCTCCACAAG-3′. All products were single bands of the expected molecular weight.

Quantitative PCR. RNA was extracted and cDNA was synthesized as described above. Taqman Gene Expression Master Mix (Applied Biosystems) was used along with Taqman probes designed against the murine Bbc3 (PUMA) mRNA sequence (Mm00519268_ml) or GAPDH mRNA (Mm99999915_gl). GAPDH mRNA was analyzed for each sample and used for comparison as an endogenous control for equal sample. All reactions were run in at least duplicate, and cDNA made from 25 ng of starting RNA template was used for each reaction. The PCR was run according to the instructions of the manufacturer, and data were quantified using the ABI Prism 7900HT Real-Time PCR system (Applied Biosystems) and SDS (Sequence Detection System) version 2.4 software (Applied Biosystems).

Hidden-platform water maze. Before training, mice were handled for 2 min/d for 5 d. The circular water-maze tank (120 cm diameter, 50 cm deep), filled to 40 cm depth with water made opaque by nontoxic white paint, was located in a dimly lit room (Teixeira et al., 2006; Maei et al., 2009; Yiu et al., 2011). Water temperature was maintained at 28 ± 1°C. A circular (5 cm radius) platform was submerged 1 cm below the water surface and in a fixed position throughout training. The pool was surrounded by white curtains painted with distinct cues, 1 m from the pool perimeter. Mice received two blocks of three trials per day, for 6 training days. At the start of each trial, mice were placed in the pool, facing the wall in one of the quadrants (north, east, south, or west). The trial was complete once the mouse found the platform or 60 s had elapsed. If the mouse failed to find the platform, it was guided by the experimenter onto the platform. After each training trial, the mouse was allowed 15 s on top of the platform. On day 1, 4 d before training sessions, and on day 7 when training was complete, spatial memory was assessed in a probe test during which the platform was removed from the pool and the mouse was allowed 60 s to search. Behavioral data from the training and probe trials were acquired and analyzed using an automated tracking system (ActiMetrics; WaterMaze). For the training data, we analyzed the escape latency and swim speed. In the probe test, the amount of time mice spent in the target zone (20 cm radius, centered on the location of the platform during training; 11% of the pool surface) versus the average time spent in the three other equivalently sized zones located in the other quadrants of the pool was measured (Moser et al., 1993; Moser and Moser, 1998; de Hoz et al., 2004). This is a sensitive measure of spatial memory.

Cued-platform water maze. Mice were trained as above (for 6 d), but the position of the platform changed for each training trial and was made visible. A red cylindrical object was placed 7 cm above the 5-cm-radius platform, which was submerged 1 cm below the water surface (as above). Two blocks of three trials were given during each training day. The time to reach the platform across training days was measured using the ActiMetrics WaterMaze software.

Standard context fear conditioning. During training, mice were placed in the training context. Two minutes later, a tone (80 dB, 2.8 kHz, 30 s) that coterminated with a footshock (0.6 mA intensity, 2 s) was delivered. Mice were returned to their home cages 1 min later. Twenty-four hours after the training session, mice were returned into the training context, and the percentage of time spent freezing for 3 min was assessed as a measure of standard context fear conditioning.

Context preexposure fear conditioning. Mice were trained as described previously (Frankland et al., 2004). Mice were randomly divided into preexposure (PE) and non-preexposure (NPE) groups. Mice in the PE group were individually placed in the conditioning chamber for 10 min. No shocks were delivered in this phase of the experiment. Mice in the NPE group remained in the home cage. Twenty-four hours later, all mice were placed in the conditioning context and, 5 s later, received an immediate footshock (2 s, 1.0 mA). Twenty-four hours after immediate shock training, mice were placed in conditioning context and freezing was assessed for a 3 min period. During this period, no shock was presented.

Open field. Mice are individually placed in a 50 × 50 × 25 cm open-field chamber for 15 min to assess locomotor and anxiety-like behavior. ActiMetrics Limelight program is a video tracker system that records the paths of animals while performing a task in a box. This program was used to analyze the distance traveled, locomotion speed, and amount of time the mice spent in respective zones (outer, middle, and center) of the box.

Antibodies. For immunostaining, the primary antibodies used were mouse anti-p63 (1:200), mouse anti-NeuN (1:500; Millipore Bioscience Research Reagents), Alexa Fluor 488-conjugated mouse anti-NeuN (1:100; Millipore), rat anti-BrdU (1:200; Accurate Chemical), rabbit anti-Sox2 (1:200; Cell Signaling Technology), goat anti-Sox2 (1:50; Santa Cruz Biotechnology), rabbit anti-GFAP (1:1000; Dako), goat anti-DCX (1:200; Santa Cruz Biotechnology), rabbit anti-CC3 (1:500; Cell Signaling Technology), chicken anti-nestin (1:1000; Aves Labs), and chicken anti-GFP (1:1000; Millipore). The secondary antibodies used for immunostaining were Alexa Fluor 555-conjugated donkey anti-mouse and anti-rabbit IgG (1:1000; Invitrogen), Alexa Fluor 488-conjugated donkey anti-mouse and anti-rabbit IgG (1:1000; Invitrogen), Alexa Fluor 488-conjugated chicken anti-rat IgG (1:1000; Invitrogen), and Cy3-conjugated donkey anti-goat antibody (1:1000; Jackson ImmunoResearch).

Statistical analyses. Statistics were performed using two-tailed Student's *t* test unless otherwise indicated. To analyze the data from the

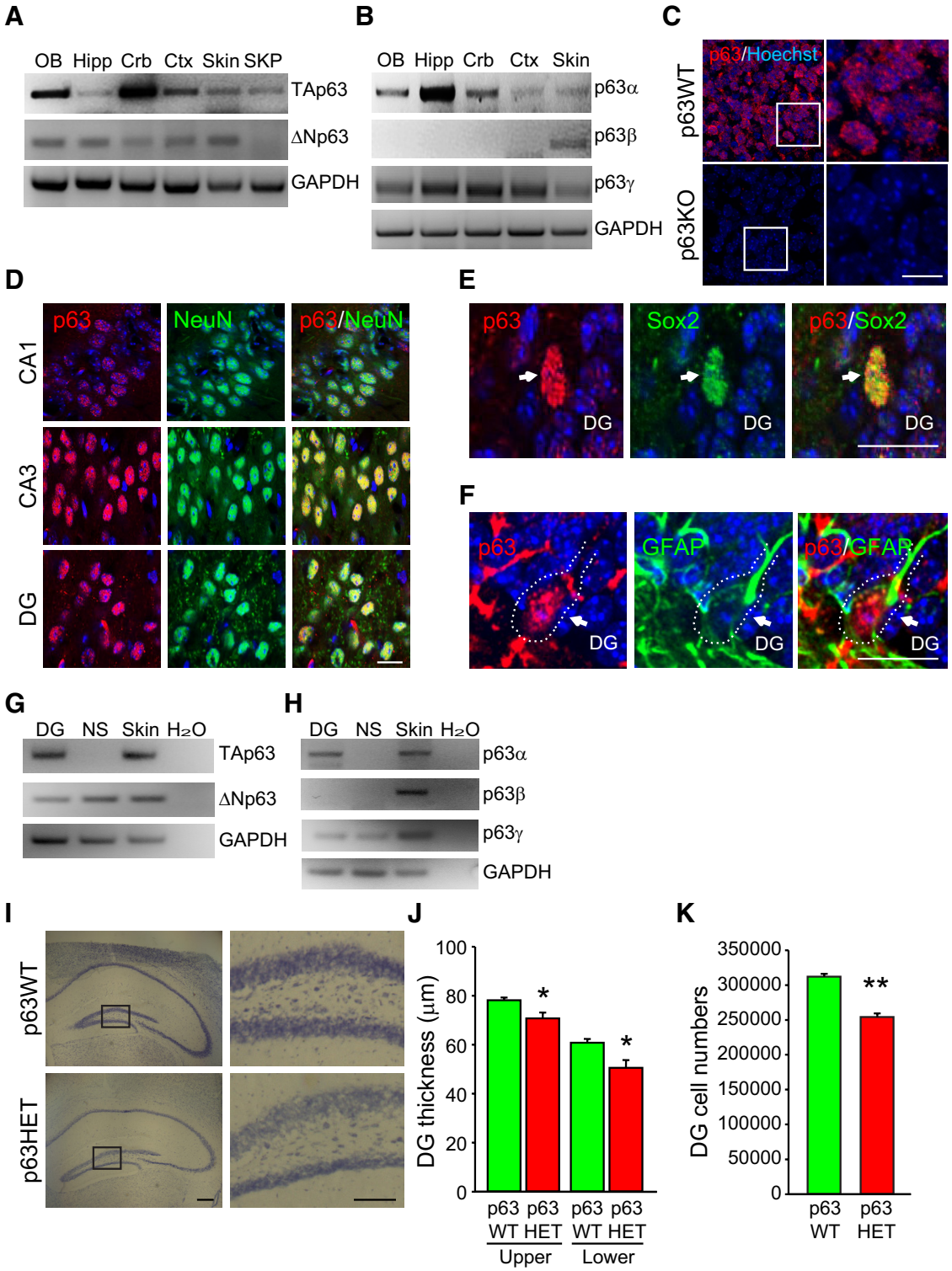

Figure 1. Expression of p63 in precursors and neurons of the adult hippocampus. ***A***, ***B***, RT-PCR analysis for TAp63 and ΔNp63 mRNA (***A***) or mRNAs encoding the C-terminal splice variants p63α, β, and γ (***B***) in total RNA from the adult murine olfactory bulb (OB), hippocampus (Hipp), cerebellum (Crb), and cortex (Ctx). Postnatal day 1 skin (Skin) and cultured dermal skin-derived precursors (SKP) were used as controls because skin expresses mRNAs for all of the p63 isoforms, whereas skin-derived precursors express TAp63 but not ΔNp63 mRNA (Su et al., 2009). The same samples were also analyzed for GAPDH mRNA. ***C***, Micrographs of embryonic day 17 cortical sections from $p63^{+/+}$ (p63WT) and $p63^{-/-}$ (p63KO) mice, immunostained with a pan-p63 antibody (red) and counterstained with Hoechst 33258 (blue) to show nuclei. Images are from the cortical plate, which contains newborn neurons. The right column shows the boxed regions in the left column at higher magnification. Scale bar, 25 μm. ***D***, Micrographs of coronal sections through the CA1 (top), CA3 (middle), and dentate gyrus (bottom) regions of the adult murine hippocampus immunostained for p63 (red) and the neuronal marker NeuN (green; the right column show the merge). Tissue was counterstained with Hoechst (blue) to show nuclei. Scale bar, 25 μm. ***E***, ***F***, High-magnification images of the SGZ of the dentate gyrus immunostained for p63 (red) and Sox2 (green, ***E***) or GFAP (green, ***F***). Sections were counterstained with Hoechst (blue) to show nuclei. Arrows denote double-labeled cells. Scale bars, 25 μm. ***G***, ***H***, RT-PCR analysis for TAp63 and ΔNp63 mRNA (***G***) or mRNAs encoding the C-terminal splice variants p63α, β, and γ (***H***) in total RNA from the adult murine dentate gyrus (DG) and neurospheres derived from the postnatal day 5 dentate gyrus (NS). ***I***, Micrographs of coronal sections of 3-month-old $p63^{+/+}$ (p63WT) and $p63^{+/-}$ (p63HET) mice at the level of the hippocampus. Scale bar, 250 μm. The right columns show higher-magnification images of the upper and lower dentate gyrus blades as indicated in the boxed areas (*Figure legend continues.*)

behavioral tasks and from the multi-group neuroanatomical studies, we used one-way ANOVA unless otherwise indicated. Significant interactions or main effects were further analyzed using Newman–Keuls *post hoc* tests. All tests were performed using Prism 5 (GraphPad Software) or Statistica. In all cases, error bars indicate SEM.

Results

Haploinsufficiency for p63 causes deficits in hippocampal NPCs and adult-born neurons

We first asked about p63 expression in the hippocampus, one of two sites of adult neurogenesis in the mammalian brain. RT-PCR analysis showed that both TAp63 and truncated ΔNp63 mRNAs were expressed in the hippocampus, olfactory bulb, cerebellum, and cortex (Fig. 1*A*). Moreover, of the p63 C-terminal variants generated by alternative splicing, p63α and p63γ but not p63β mRNAs were expressed in these same regions (Fig. 1*B*). To ask which hippocampal cell types expressed p63, we performed immunocytochemistry with a well-characterized pan-p63 antibody (4A4) after first confirming that it immunostained cells in the cortex of $p63^{+/+}$ but not $p63^{-/-}$ embryos (Fig. 1*C*). We observed broad p63 immunoreactivity in NeuN-positive hippocampal neurons (Fig. 1*D*). Furthermore, p63 immunoreactivity was detected in the SGZ of the dentate gyrus in NeuN-negative cells that coexpressed the neural precursor markers Sox2 (Fig. 1*E*) and GFAP (Fig. 1*F*). Quantification showed that ~37% of Sox2-positive precursors expressed detectable p63. To confirm that p63 is expressed by hippocampal precursors, we cultured neonatal dentate gyrus precursors as neurospheres and performed RT-PCR; these neurospheres expressed ΔNp63 but not detectable TAp63 (Fig. 1*G*), and of the C-terminal variants, they expressed p63γ (Fig. 1*H*).

We next asked whether p63 was functionally important in the hippocampus. Because $p63^{-/-}$ mice die at birth (Mills et al., 1999), we examined $p63^{+/-}$ mice and asked whether there were any obvious deficits in hippocampal structure. Nissl staining demonstrated that overall hippocampal morphology was normal in the $p63^{+/-}$ mice but that there was a statistically significant decrease in thickness of the upper and lower blades of the dentate gyrus relative to their $p63^{+/+}$ littermates (Fig. 1*I*,*J*). To ask whether this reflected a decrease in neurons, we measured the density of granule neurons and total dentate gyrus area. Quantification of 10 sections sampled throughout the rostrocaudal extent of the hippocampus showed that granule neuron density was similar in mice of both genotypes ($p63^{+/+}$ cell density, 0.0199 ± 0.0005 cells per μm^2; $p63^{+/-}$ cell density, 0.0193 ± 0.0015 cells per μm^2; $p > 0.05$) but that there was a decrease in total dentate gyrus area ($p63^{+/+}$ area, 156,612 ± 2052 μm^2; $p63^{+/-}$ area, 131,432 ± 2796 μm^2; $p = 0.0019$), and thus total number of granule neurons (Fig. 1*K*), in $p63^{+/-}$ mice.

One cellular perturbation that can result in fewer dentate gyrus neurons is decreased adult neurogenesis. Therefore, we asked whether p63 haploinsufficiency affected hippocampal NPCs. Initially, we characterized the number of proliferating precursors in the dentate gyrus by administering BrdU to 3-month-old $p63^{+/-}$ mice. Immunostaining (Fig. 2*A*) and quantitative analysis 1 d after BrdU administration showed an almost twofold decrease in the number of BrdU-positive SGZ precursors in $p63^{+/-}$ mice (Fig. 2*B*). To ask whether this phenotype reflected a decrease in hippocampal precursors, we quantified the number of cells expressing the pan-precursor marker Sox2. Like the BrdU data, this analysis demonstrated a significant decrease in NPCs in $p63^{+/-}$ mice (Fig. 2*C*). Moreover, quantification of the proportion of Sox2-positive cells that were also BrdU positive demonstrated that there was a decrease in total double-labeled cells in $p63^{+/-}$ mice (Fig. 2*D*). However, the proliferation index (the proportion of total Sox2-positive cells that were also BrdU-positive) was similar in both groups [12.6% in wild type (WT) mice vs 11.9% in $p63^{+/-}$ mice], suggesting that p63 haploinsufficiency causes a decrease in hippocampal NPCs but that it does not affect their rate of proliferation.

To ask whether this decrease in SGZ NPCs in $p63^{+/-}$ mice was coincident with a decrease in the number of adult-born neurons, we administered BrdU and then analyzed BrdU-positive dentate gyrus neurons 30 d later by immunostaining for BrdU and the neuronal marker NeuN (Fig. 2*E*). Quantification showed that the dentate gyrus of $p63^{+/+}$ mice contained 1537 ± 23 total BrdU-positive cells, and, of these, 1460 ± 36, or ~90–95%, were double labeled for NeuN. In contrast, the dentate gyrus of $p63^{+/-}$ mice contained 960 ± 10 total BrdU-positive cells, and, of these, 863 ± 37, or 90–95%, were NeuN positive. Thus, although the ratio of BrdU-positive cells that were NeuN positive was similar in both genotypes, $p63^{+/-}$ mice had ~40% fewer adult-born hippocampal neurons than did their WT $p63^{+/+}$ littermates (Fig. 2*F*). Immunostaining for DCX (Fig. 2*G*), which is transiently expressed in newborn neurons, supported this conclusion, because quantification showed that the number of DCX-positive cells was also decreased in $p63^{+/-}$ mice (Fig. 2*H*).

These data suggest that p63 is essential to maintain normal numbers of hippocampal NPCs and adult-born neurons. To ask whether p63 does this by promoting cell survival, we immunostained hippocampal sections from 3-month-old mice for the apoptotic protein CC3 and either the precursor marker Sox2 (Fig. 2*I*) or the newborn neuron marker DCX (Fig. 2*K*). Quantification of total double-labeled cells on 10 sections sampled throughout the rostrocaudal extent of the hippocampus showed that ~13% of Sox2-positive SGZ cells were also positive for CC3 in the $p63^{+/+}$ dentate gyrus and that this doubled to ~26% in $p63^{+/-}$ mice (Fig. 2*J*). Similarly, although ~12% of WT newborn neurons were CC3 positive, this was almost doubled in $p63^{+/-}$ mice (Fig. 2*L*). To confirm this apoptotic phenotype, we performed TUNEL assays for DNA fragmentation resulting from apoptosis on similar sections (Fig. 2*M*). Approximately 8% of WT Sox2-positive cells were TUNEL positive, and this was increased almost threefold in the $p63^{+/-}$ dentate gyrus (Fig. 2*N*). Thus, haploinsufficiency for p63 causes a decrease in neural precursors and newly born neurons, at least in part as a consequence of enhanced apoptosis.

p63 also regulates the number of adult forebrain NPCs and adult-born olfactory neurons

To assess whether p63 generally regulates the numbers of adult neural precursors and adult-born neurons, we examined NPCs of the forebrain SVZ that generate new interneurons for the adult olfactory bulb. Initially, we characterized p63 expression. RT-PCR demonstrated that both TAp63 and ΔNp63 mRNAs were expressed, as were the mRNAs for the p63α and p63γ isoforms (Fig. 3*A*,*B*). We also analyzed SVZ precursors that had been cul-

←

(*Figure legend continued.*) in the left column. Scale bar, 100 μm. ***J***, Quantification of the mean thickness of the upper and lower blades of the dentate gyrus (in micrometers) as determined from sections similar to those in ***I***. $^*p < 0.05$; $n = 3$ animals per group. ***K***, Quantification of total dentate gyrus granule cell numbers in p63WT versus p63HET mice as determined by measuring neuronal density and total dentate gyrus area in 10 sections spanning the rostrocaudal extent of the hippocampus similar to those in ***I***. $^{**}p < 0.01$; $n = 3$ animals per group. In all panels, error bars denote SEM.

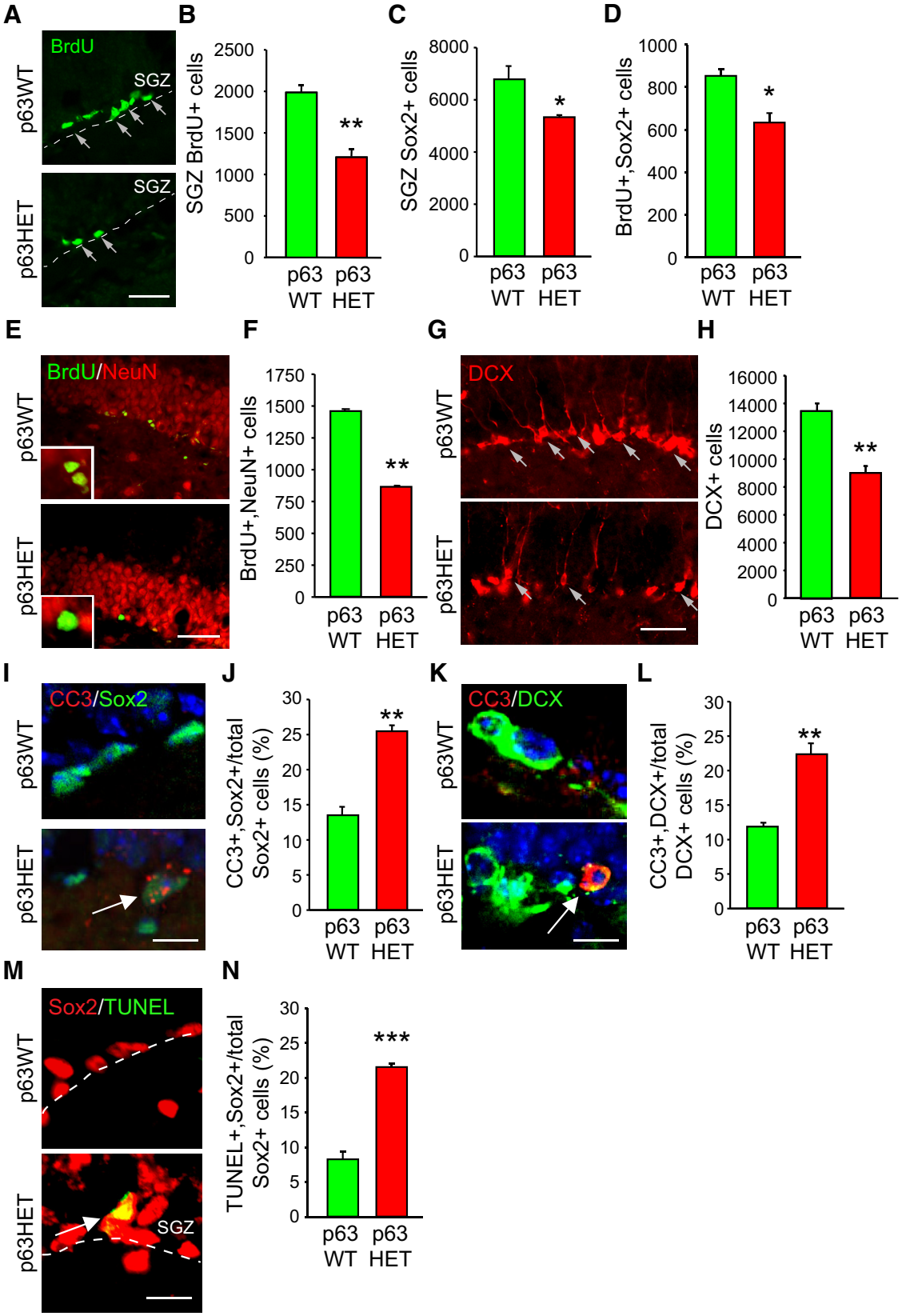

Figure 2. Adult NPCs and adult-born neurons are reduced in the SGZ of 3-month-old $p63^{+/-}$ mice. *A*, Coronal sections through the SGZ of the $p63^{+/+}$ (p63WT) and $p63^{+/-}$ (p63HET) dentate gyrus immunostained for BrdU (green) 1 d after BrdU injection. The dotted line denotes the boundary between the blade of the dentate gyrus and the hilus, and arrows denote positive cells. Scale bar, 50 μm. ***B***, Quantification of the total number of BrdU-positive SGZ cells as determined by counting 10 sections spanning the rostrocaudal extent of the hippocampus similar to those seen in ***A***. $^{**}p < 0.01$; $n = 3$ animals each. ***C***, Quantification of the total number of Sox2-positive cells in the SGZ of adult $p63^{+/+}$ (p63WT) and $p63^{+/-}$ (p63HET) mice determined as in ***B***. $^{*}p < 0.05$; $n = 3$ animals each. ***D***, Quantification of the total number of BrdU-positive, Sox2-positive cells in the SGZ of adult $p63^{+/+}$ (p63WT) and $p63^{+/-}$ (p63HET) mice determined as in ***B***. $^{*}p < 0.05$; $n = 3$ animals each. ***E***, Micrographs of coronal sections through the dentate gyrus of $p63^{+/+}$ (p63WT) and $p63^{+/-}$ (p63HET) mice that were injected with BrdU at 2 months (*Figure legend continues.*)

tured as neurospheres; RT-PCR showed that, like the dentate gyrus neurospheres, SVZ neurospheres expressed ΔNp63 but not detectable TAp63 mRNA (Fig. 3*A*,*B*). To confirm that SVZ neural precursors expressed p63, we immunostained coronal cortical sections at the level of the SVZ from 3-month-old mice with anti-pan-p63 and either anti-NeuN (Fig. 3*C*) or antibodies for the adult precursor markers nestin (Fig. 3*D*), GFAP (Fig. 3*E*), or Sox2 (data not shown). p63 immunoreactivity was detectable in most NeuN-positive cortical neurons. For example, ~96% of cortical neurons in layers III/IV expressed detectable p63 immunoreactivity. Moreover, p63 was detectable in many SVZ cells that expressed nestin, GFAP, or Sox2. Quantification showed that ~32% of Sox2-positive SVZ cells expressed detectable p63.

To ask whether p63 haploinsufficiency regulated the number of adult-born olfactory neurons, we treated 2-month-old $p63^{+/-}$ and $p63^{+/+}$ mice with BrdU and, 30 d later, sectioned the entirety of the olfactory bulb and quantified the number of BrdU-positive, NeuN-positive neurons (Fig. 3*F*). This analysis demonstrated a 40% decrease in adult-born olfactory neurons in $p63^{+/-}$ mice (Fig. 3*G*). To ask whether there were also changes in neural precursors, we treated 3-month-old mice with BrdU and 1 d later sectioned the SVZ and quantified the proportion of Sox2-positive precursors in the SVZ that were BrdU positive (Fig. 3*H*). Quantification of the total number of double-labeled cells in 10 sections sampled throughout the SVZ showed that there was an ~20% decrease in proliferating Sox2-positive neural precursors in the $p63^{+/-}$ SVZ (Fig. 3*I*). To ask whether this reflected a decrease in total SVZ precursors, we dissected the SVZ and cultured the cells under clonal neurosphere conditions (Fig. 3*J*); the $p63^{+/-}$ SVZ contained approximately half as many neurosphere-initiating cells as did the $p63^{+/+}$ SVZ (Fig. 3*K*). To ask whether this decrease in proliferating neural precursors might be attributable, in part, to increased apoptosis, as seen in the SGZ, we immunostained 10 sections through the SVZ for Sox2 and either CC3 immunostaining or TUNEL staining and determined the proportion of double-labeled cells (Fig. 3*L*,*N*). This analysis demonstrated a significant twofold increase in the proportion of Sox2-positive cells that were positive for either CC3 or TUNEL (Fig. 3*M*,*O*), consistent with enhanced precursor death.

Acute conditional deletion of p63 in adult neural precursors causes apoptosis and depletion of precursor pools

To ask whether these deficits in neural precursors and adult-born neurons in $p63^{+/-}$ mice reflected a cell-autonomous requirement for p63, we acutely ablated p63 in adult neural precursors. $p63^{fl/fl}$ mice (Mills et al., 2002) were crossed to mice carrying a *nestin–CreERT2* transgene (Imayoshi et al., 2008) and a floxed YFP reporter gene in the Rosa26 locus (Lagace et al., 2007) to monitor successful Cre-mediated recombination. We then treated 2-month-old $p63^{fl/fl}$;*nestin–CreERT2*$^{+/\varnothing}$;$Rosa26R^{YFP/YFP}$ mice with tamoxifen to inducibly delete p63. $p63^{+/+}$;*nestin–CreERT2*$^{+/\varnothing}$;$Rosa26R^{YFP/YFP}$ mice were used as controls. Both groups of mice were treated for three cycles of tamoxifen treatment (five daily injections followed by 3 weeks with no tamoxifen), and mice were examined neuroanatomically at 5 months of age. To confirm that this protocol resulted in inducible Cre-mediated recombination in adult neural precursors, as reported previously (Imayoshi et al., 2008; Arruda-Carvalho et al., 2011), we examined YFP immunostaining in coronal sections at the level of the hippocampus. Quantification of total YFP-positive cells in 10 sections spanning the rostrocaudal extent of the hippocampus demonstrated that YFP-positive cells were present in the SGZ, consistent with previous studies using this *nestin–CreERT2* mouse line (Imayoshi et al., 2008; Arruda-Carvalho et al., 2011) but that they were decreased by almost half in $p63^{fl/fl}$;*nestin–CreERT2*$^{+/\varnothing}$;$Rosa26R^{YFP/YFP}$ mice relative to controls (Fig. 4*A*,*B*). To determine whether this reflected a decrease in YFP-positive precursors and/or neurons, we performed double-labeled immunostaining. Analysis of total double-labeled cells in 10 hippocampal sections demonstrated a 50% decrease in YFP-positive SGZ precursors that expressed Sox2 (Fig. 4*C*) or GFAP (Fig. 4*D*) and in dentate gyrus neurons that coexpressed DCX (Fig. 4*E*) or NeuN (Fig. 4*F*). To confirm that these numbers reflected a decrease in precursors and neurons, and not just alterations in YFP expression, we counted total Sox2-positive and DCX-positive cells in 10 similar sections of the SGZ. Both precursors and newborn neurons were significantly decreased in the dentate gyrus of $p63^{fl/fl}$;*nestin–CreERT2*$^{+/\varnothing}$;$Rosa26R^{YFP/YFP}$ mice relative to $p63^{+/+}$;*nestin–CreERT2*$^{+/\varnothing}$;$Rosa26R^{YFP/YFP}$ controls (Fig. 4*G*,*H*). We also quantified the total number of new neurons by injecting these mice with BrdU at 4 months of age and analyzing total BrdU-positive, NeuN-positive granule cells 1 month later at 5 months; analysis of 10 sections sampled throughout the hippocampus demonstrated that adult-born neurons were decreased by ~40% in the $p63^{fl/fl}$;*nestin–CreERT2*$^{+/\varnothing}$;$Rosa26R^{YFP/YFP}$ mice (Fig. 4*I*).

These data indicate that genetic ablation of p63 in adult hippocampal neural precursors and their adult-born progeny ultimately causes decreases in both cell populations. To ask whether this was also true for the SVZ, we examined YFP immunostaining in coronal sections at the level of the lateral ventricles of these same two groups of mice. We observed many YFP-positive cells in the SVZ and rostral migratory stream of both genotypes, but there were apparently fewer YFP-positive cells in the $p63^{fl/fl}$;*nestin–CreERT2*$^{+/\varnothing}$;$Rosa26R^{YFP/YFP}$ SVZ (Fig. 4*J*). To confirm that this reflected a decrease in SVZ precursors, we dissected the SVZ and cultured the cells under clonal neurosphere conditions. The SVZ of $p63^{fl/fl}$;*nestin–CreERT2*$^{+/\varnothing}$;$Rosa26R^{YFP/YFP}$ mice contained less than half as many neurosphere-initiating cells (Fig. 4*K*). To ask whether there was also a decrease in adult-born neurons, we injected both groups of mice with BrdU at 4 months of age and analyzed the olfactory bulb 1 month later at 5 months. Immunostaining and quantification of 10 sections spanning the entirety of the olfactory bulb showed that $p63^{fl/fl}$;*nestin–CreERT2*$^{+/\varnothing}$;$Rosa26R^{YFP/YFP}$ mice had only approximately half as many BrdU-positive, NeuN-positive adult-born neurons as did $p63^{+/+}$;*nestin–CreERT2*$^{+/\varnothing}$;$Rosa26R^{YFP/YFP}$ controls (Fig. 4*L*).

←

(*Figure legend continued.*) of age and analyzed 1 month later at 3 months, immunostained for BrdU (green) and NeuN (red). The insets show double-labeled cells at higher magnification. Scale bar, 100 μm. ***F***, Quantification of the total number of BrdU-positive, NeuN-positive granule cells in the dentate gyrus, determined by counting 10 sections similar to those in ***E*** spanning the rostrocaudal extent of the hippocampus. $^{**}p < 0.01$; $n = 3$ animals each. ***G***, Micrographs of coronal sections through the $p63^{+/+}$ (p63WT) and $p63^{+/-}$ (p63HET) dentate gyrus, immunostained for DCX (red). Arrows denote DCX-positive cells. Scale bar, 100 μm. ***H***, Quantification of the total number of DCX-positive newborn neurons in the dentate gyrus, determined by counting 10 sections similar to those in ***G*** spanning the rostrocaudal extent of the hippocampus. $^{**}p < 0.01$; $n = 3$ animals each. ***I–L***, Coronal sections through the $p63^{+/+}$ (p63WT) and $p63^{+/-}$ (p63HET) SGZ were immunostained for CC3 (red, ***I***, ***K***) and Sox2 (green, ***I***) or DCX (green, ***K***), and the total number of double-positive cells were determined by counting 10 sections sampled throughout the rostrocaudal extent of the hippocampus (***J***, ***L***). In ***I*** and ***K***, sections were counterstained with Hoechst (blue), and arrows denote double-labeled cells. $^{**}p < 0.01$; $n = 3$ animals each; 80–374 total double-labeled cells per hippocampus were counted. Scale bar, 50 μm. ***M***, ***N***, Coronal sections through the $p63^{+/+}$ (p63WT) and $p63^{+/-}$ (p63HET) SGZ were sampled as in ***I*** and ***K***, immunostained for TUNEL (green) and Sox2 (red) (***M***), and double-positive cells were quantified (***N***). Arrow denotes a double-labeled cell. $^{***}p < 0.001$; $n = 3$ animals each; 60–116 total double-labeled cells per hippocampus were counted. Scale bar, 50 μm. In all panels, error bars denote SEM.

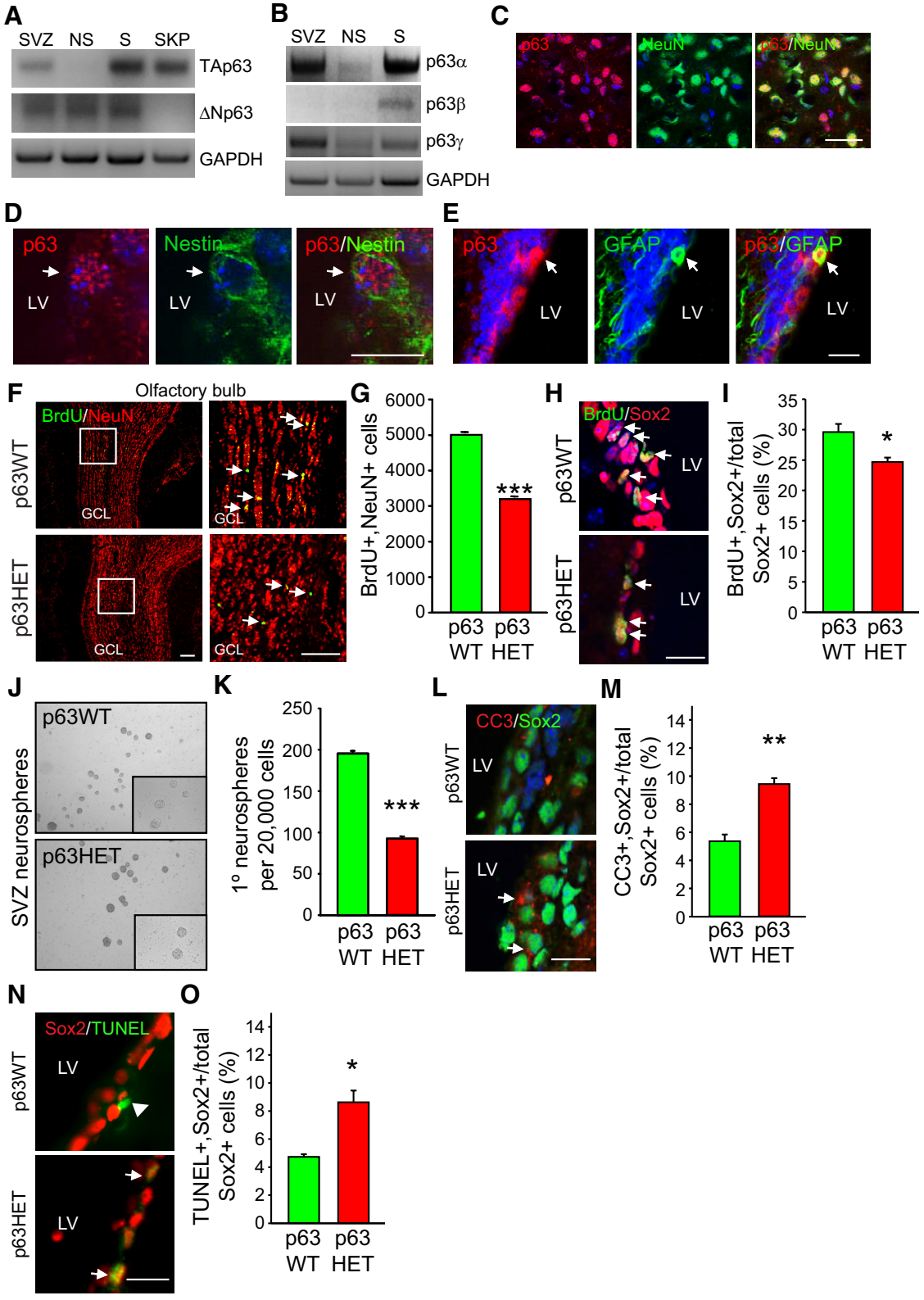

Figure 3. p63 haploinsufficiency causes decreased SVZ NPCs and decreased adult-born olfactory neurons in 3-month-old mice. ***A***, ***B***, RT-PCR analysis for TAp63 and ΔNp63 mRNA (***A***) or mRNAs encoding the C-terminal splice variants p63α, β, and γ (***B***) in total RNA from the adult SVZ or from cultured adult SVZ neurospheres (NS). Postnatal day 1 skin (S) and cultured dermal skin-derived precursors (SKP) were used as controls because skin expresses mRNAs for all of the p63 isoforms, whereas SKPs express TAp63 but not ΔNp63 mRNA. The same samples were also analyzed for GAPDH mRNA. ***C***, Micrographs of a coronal cortical section immunostained for p63 (red) and NeuN (green; the far right panel is the merge). The section was counterstained with Hoechst (blue). Scale bar, 50 μm. ***D***, ***E***, Micrographs of coronal sections through the SVZ immunostained for p63 (red) and nestin (green, ***D***) or GFAP (green, ***E***). Sections were counterstained with Hoechst 33258 (blue). LV denotes the lateral ventricle and arrows double-labeled cells. Scale bar, 25 μm. ***F***, Micrographs of coronal sections through the $p63^{+/+}$ (p63WT) and $p63^{+/-}$ (p63HET) olfactory bulb 30 d after BrdU injection, immunostained for BrdU (green) and NeuN (red). The boxed areas in the left column are shown at higher magnification in the right column. Arrows denote double-labeled cells. Scale bar, 200 μm. ***G***, Quantification of the total number of BrdU-positive, NeuN-positive olfactory bulb neurons, as determined by analyzing 10 sections spanning the extent of the (*Figure legend continues.*)

The ΔNp63 isoform promotes survival of adult neural precursors via a p53 and PUMA-dependent mechanism

Together, these data indicate that genetic ablation of p63 in adult neural precursors causes depletion of precursors and newborn neurons and that it likely does so, at least in part, by causing cell death. To confirm this conclusion and to ask about the underlying cellular mechanisms, we turned to culture studies, focusing on adult SVZ precursors, which can be cultured as neurospheres. Initially, we performed experiments to definitively test the idea that p63 was essential for adult neural precursor survival by culturing SVZ neurospheres from *nestin–CreERT2*$^{+/\varnothing}$;*Rosa26R*$^{YFP/YFP}$ mice that were either *p63*$^{fl/fl}$ or *p63*$^{+/+}$ but that had not been treated with tamoxifen *in vivo*. These neurospheres were passaged, various concentrations of tamoxifen were added to the cultures 2 d later, and cells were immunostained for YFP and CC3 after an additional 2 d in culture (Fig. 5*A*). The activation of Cre recombinase by tamoxifen addition in culture resulted in apoptosis of more than half the YFP-positive *p63*$^{fl/fl}$ but not *p63*$^{+/+}$ neurosphere cells, and this effect was dose dependent (Fig. 5*B*).

These results show an ongoing requirement for p63 in survival of adult neural precursors. To ask which p63 isoforms were necessary for neural precursor survival, we expressed Cre recombinase in cultured SVZ cells from mice carrying floxed alleles of p63, TAp63, or ΔNp63 (Mills et al., 2002; Su et al., 2009). SVZ cells were cultured and transduced with recombinant adenovirus expressing EGFP or Cre recombinase, and neurosphere numbers were quantified. When *p63*$^{+/+}$ cultures were transduced with either EGFP or Cre recombinase, neurosphere numbers were similar to control, nontransduced cultures (Fig. 5*C*). Similarly, the number of neurospheres generated from *p63*$^{fl/fl}$ cells was unaffected by transduction with EGFP (Fig. 5*D*). However, when *p63*$^{fl/fl}$ cultures were transduced with Cre recombinase, neurosphere numbers were reduced by twofold (Fig. 5*D*), as predicted by the tamoxifen experiment (Fig. 5*A*,*B*). A similar reduction in neurosphere number was observed when ΔN*p63*$^{fl/fl}$, but not TA*p63*$^{fl/fl}$, cultures were transduced with Cre recombinase adenovirus versus EGFP adenovirus (Fig. 5*E*,*F*), indicating that the ΔNp63 isoform was responsible for maintaining precursor survival. To confirm that the decrease in neurosphere number seen after acute ablation of ΔNp63 was attributable to cell death, we performed similar experiments with and without the addition of the pan-caspase inhibitor ZVAD. Acute ablation of ΔNp63 with Cre recombinase caused a significant decrease in neurospheres, and this was rescued by ZVAD (Fig. 5*G*). Thus, ΔNp63 is essential for survival of cultured adult SVZ neural precursors.

One way ΔNp63 regulates survival is by antagonizing p53 (Yang and McKeon, 2000), and p53 has been shown to cause apoptosis of adult SVZ neural precursors (Meletis et al., 2006). To ask whether ΔNp63 promotes precursor survival by antagonizing p53, we used a lentivirus expressing p53 shRNA to suppress p53 levels. Initially, we confirmed the efficacy of this shRNA; WT neurospheres were transduced with lentiviruses expressing either scrambled or p53 shRNAs, and then 4 d later, we performed RT-PCR for p53 mRNA or, as controls, p63, p73, and GAPDH mRNAs. The p53 shRNA reduced the levels of p53 mRNA without affecting those of the other family members (Fig. 5*H*). Having confirmed the efficacy of this shRNA, we asked whether coincident knockdown of p53 could rescue the enhanced cell death seen when ΔNp63 was genetically ablated. Specifically, we transduced ΔN*p63*$^{+/+}$ and ΔN*p63*$^{fl/fl}$ SVZ cells with a Cre recombinase lentivirus with or without the p53 shRNA lentivirus and quantified neurosphere number 6 d later. As seen in the adenovirus experiments, transduction with Cre recombinase significantly reduced the number of neurospheres generated from ΔN*p63*$^{fl/fl}$ (Fig. 5*I*), but not ΔN*p63*$^{+/+}$, cells (data not shown). Moreover, coincident transduction with p53 shRNA significantly rescued this decrease (Fig. 5*I*). Thus, ΔNp63 promotes the maintenance of normal numbers of adult neural precursors, and it does this, at least in part, by antagonizing p53.

Previous work has shown that the BH3-only pro-apoptotic protein PUMA acts downstream of p53 in several adult stem cell populations (Liu et al., 2010). To ask whether PUMA is also involved in the cell death that occurs in response to decreased p63 levels, we cultured neurospheres from the SVZ of adult *p63*$^{+/+}$ versus *p63*$^{+/-}$ mice and performed quantitative real-time PCR for PUMA mRNA. This analysis demonstrated that PUMA mRNA levels were significantly upregulated in *p63*$^{+/-}$ neurospheres (Fig. 5*J*). Therefore, we asked whether coincident knockdown of PUMA could rescue the neural precursor death that occurred after p63 ablation. To do this, we first validated a lentivirally driven PUMA shRNA; when expressed in WT neurospheres, the PUMA shRNA caused a decrease in PUMA mRNA but not the mRNAs for p53, p63, or p73 (Fig. 5*H*). We then transduced SVZ cells from adult *p63*$^{fl/fl}$ mice with a lentivirus expressing Cre recombinase with or without a lentivirus expressing either scrambled or PUMA shRNAs. As additional controls, we transduced the SVZ cells with an EGFP-expressing lentivirus together with either a scrambled or PUMA shRNA lentivirus. Quantification of neurosphere numbers 6 d later showed that, as predicted, expression of Cre recombinase and subsequent genetic ablation of p63 caused a decrease in neurosphere numbers, and this was rescued by the PUMA shRNA but not the scrambled shRNA (Fig. 5*K*).

The decrease in neural precursors and adult-born neurons in *p63*$^{+/-}$ mice is rescued by coincident ablation of p53 in vivo

These data support the idea that loss of p63 causes neural precursor death by a p53–PUMA-dependent mechanism in culture. To ask whether this was also true *in vivo*, we crossed the *p63*$^{+/-}$ mice with mice lacking p53 (Jacks et al., 1994) and asked whether this rescued the neural precursor phenotypes observed in the former. Initially, we focused on the hippocampus, characterizing four different genotypes: *p63*$^{+/+}$;*p53*$^{+/+}$ (WT), *p63*$^{+/+}$;*p53*$^{-/-}$ (p53KO), *p63*$^{+/-}$;*p53*$^{+/+}$, and *p63*$^{+/-}$;*p53*$^{-/-}$. Nissl staining demonstrated that hippocampal morphology was apparently similar between all of these genotypes (Fig. 6*A*). In contrast, immunostaining demonstrated that p53KOs had a small but significant increase in Sox2-positive precursors and DCX-positive

←

(*Figure legend continued.*) olfactory bulb similar to those in ***F***. GCL, Granule cell layer. ***$p <$ 0.001; $n = 3$ animals each. ***H***, Coronal sections through the SVZ of *p63*$^{+/+}$ (p63WT) and *p63*$^{+/-}$ (p63HET) mice immunostained for BrdU (green) and Sox2 (red) 1 d after BrdU injection. Arrows denote positive cells. Scale bar, 50 μm. ***I***, Quantification of the proportion of Sox2-positive cells that are also positive for BrdU in 10 sections similar to those in ***H***. *$p < 0.05$; $n = 3$ animals each; 611–955 total double-labeled cells per SVZ were counted. ***J***, ***K***, SVZ cells from 3-month-old *p63*$^{+/+}$ (p63WT) and *p63*$^{+/-}$ (p63HET) mice were dissected, cultured as primary neurospheres (***J***), and quantified (***K***). ***$p < 0.001$; $n = 3$ animals cultured individually, each in triplicate; similar results were obtained in independent experiments. ***L–O***, Coronal sections through the *p63*$^{+/+}$ (p63WT) and *p63*$^{+/-}$ (p63HET) SVZ were immunostained for Sox2 (green, ***L***; red, ***N***) and CC3 (red, ***L***) or TUNEL (green, ***N***), and the proportion of Sox2-positive cells that were double labeled for CC3 (***M***) or TUNEL (***O***) was quantified. Arrows denote double-labeled cells and the arrowhead (***N***) a TUNEL-positive, Sox2-negative cell. *$p < 0.05$, **$p <$ 0.01; $n = 3$ animals per group; 142–265 total double-labeled cells per SVZ were counted for the Sox2 analysis and 137–259 for the TUNEL analysis. Scale bar, 50 μm. In all panels, error bars denote SEM.

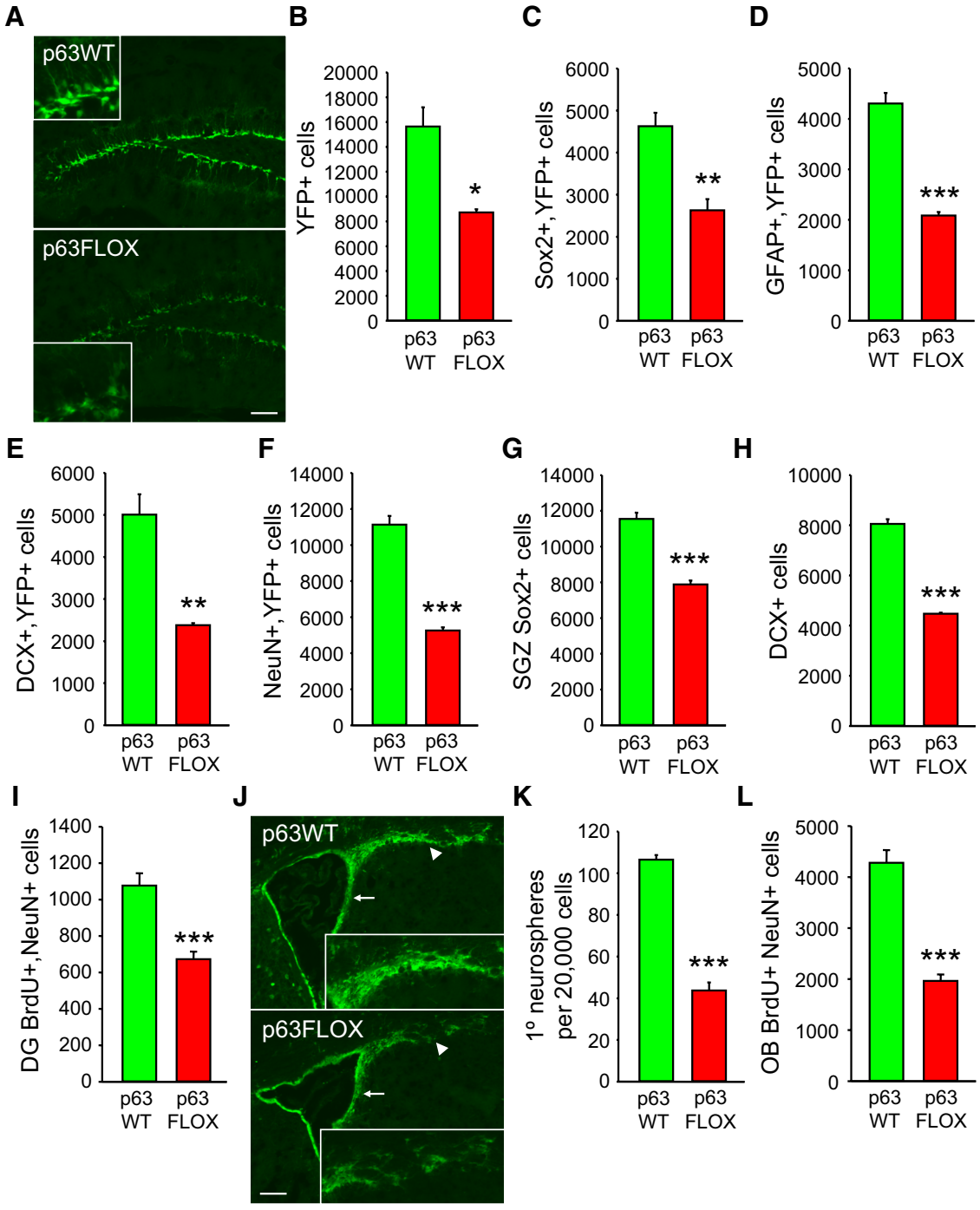

Figure 4. Acute ablation of p63 in adult $p63^{fl/fl}$;*nestin–CreERT2*$^{+/\emptyset}$;$Rosa26R^{YFP/YFP}$ mice reduces numbers of NPCs and adult-born neurons at 5 months of age. ***A–I***, $p63^{+/+}$;*nestin–CreERT2*$^{+/\emptyset}$;$Rosa26R^{YFP/YFP}$ (p63WT) and $p63^{fl/fl}$;*nestin–CreERT2*$^{+/\emptyset}$;$Rosa26R^{YFP/YFP}$ (p63FLOX) mice were treated with tamoxifen over the course of 3 months commencing at 2 months, and coronal sections at the level of the dentate gyrus were analyzed by immunostaining for YFP (***A***, insets show the SGZ at higher magnification) and/or markers for precursors or neurons. Ten sections spanning the rostrocaudal extent of the dentate gyrus were counted to determine the total number of YFP-positive cells (***B***) or YFP-positive cells that also expressed Sox2 (***C***), GFAP (***D***), DCX (***E***), or NeuN (***F***). Similar sections were also analyzed for total Sox2-positive cells within the SGZ (***G***) or total DCX-positive cells in the dentate gyrus (***H***). $*p < 0.05$, $**p < 0.01$, $***p < 0.01$; $n = 3$ animals per group. ***I***, Quantification of BrdU-positive, NeuN-positive cells in the dentate gyrus of $p63^{+/+}$;*nestin–CreERT2*$^{+/\emptyset}$;$Rosa26R^{YFP/YFP}$ (p63WT) and $p63^{fl/fl}$;*nestin–CreERT2*$^{+/\emptyset}$;$Rosa26R^{YFP/YFP}$ (p63FLOX) mice. Mice were treated with tamoxifen over the course of 3 months commencing at 2 months of age, were injected with BrdU at 4 months of age, and were analyzed 1 month later at 5 months. $***p < 0.001$; $n = 3$ animals per group. ***J***, Coronal forebrain sections at the level of the SVZ (arrows) and rostral migratory stream (arrowheads) from $p63^{+/+}$;*nestin–CreERT2*$^{+/\emptyset}$;$Rosa26R^{YFP/YFP}$ (p63WT) and $p63^{fl/fl}$;*nestin–CreERT2*$^{+/\emptyset}$;$Rosa26R^{YFP/YFP}$ (p63FLOX) mice that were treated with tamoxifen to knock-out p63 and knock-in the YFP reporter (green). Insets show the rostral migratory stream at higher magnification. Scale bar, 200 μm. ***K***, Quantification of primary neurospheres generated from 20,000 SVZ cells from $p63^{+/+}$;*nestin–CreERT2*$^{+/\emptyset}$;$Rosa26R^{YFP/YFP}$ (p63WT) and $p63^{fl/fl}$;*nestin–CreERT2*$^{+/\emptyset}$;$Rosa26R^{YFP/YFP}$ (p63FLOX) mice that were treated with tamoxifen from 2 to 5 months of age. $***p < 0.001$; $n = 6$ animals per group, two independent experiments; cells from each animal were plated independently in triplicate. ***L***, Quantification of the total number of BrdU-positive, NeuN-positive cells as determined by analyzing 10 sections spanning the entirety of the olfactory bulb of $p63^{+/+}$;*nestin–CreERT2*$^{+/\emptyset}$;$Rosa26R^{YFP/YFP}$ (p63WT) and $p63^{fl/fl}$;*nestin–CreERT2*$^{+/\emptyset}$;$Rosa26R^{YFP/YFP}$ (p63FLOX) mice. Mice were treated with tamoxifen over the course of 3 months, were injected with BrdU at 4 months of age, and were analyzed at 5 months. $***p < 0.001$; $n = 3$ animals per group. In all panels, error bars denote SEM.

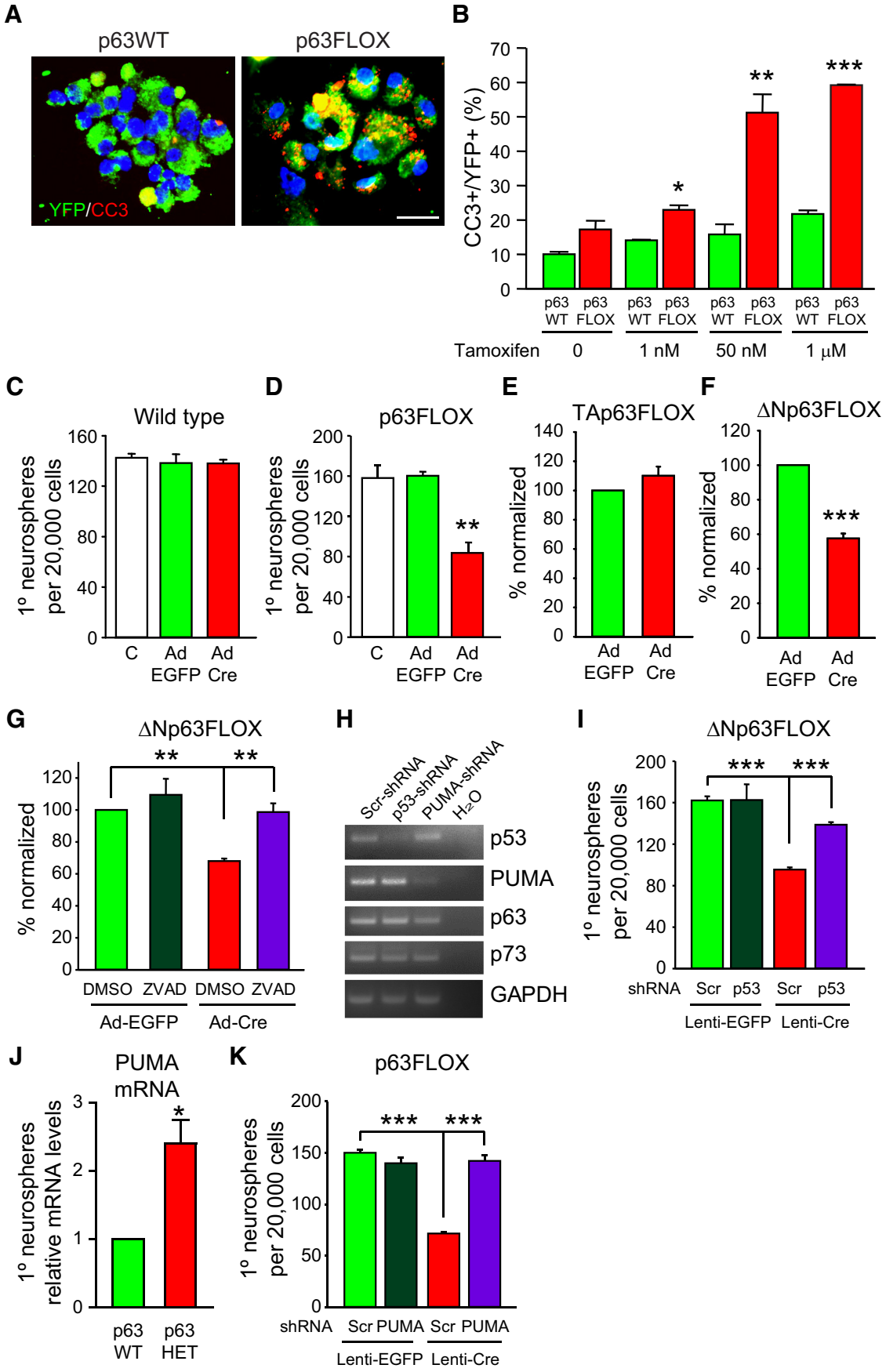

Figure 5. ΔNp63 promotes survival and maintenance of cultured SVZ neurosphere-initiating cells by repressing a p53–PUMA pathway. ***A***, ***B***, *p63*$^{+/+}$;*nestin–CreERT2*$^{+/\emptyset}$;*Rosa26R*$^{YFP/YFP}$ (p63WT) and *p63*$^{fl/fl}$;*nestin–CreERT2*$^{+/\emptyset}$;*Rosa26R*$^{YFP/YFP}$ (p63FLOX) SVZ primary neurospheres were passaged and treated with 1 nM to 1 μM tamoxifen for 2 d (***A*** shows (*Figure legend continues.*)

newborn neurons in the dentate gyrus compared with WT mice (Fig. 6*B*,*C*). Moreover, coincident p53 ablation significantly rescued the deficits in SGZ precursors and newborn neurons observed in the $p63^{+/-}$ mice (Fig. 6*B*,*C*). To confirm these findings, we administered BrdU and 1 d later performed double-label immunocytochemistry for BrdU and Sox2. There was a small but significant increase in proliferating precursors in p53KOs, and p53 ablation completely rescued the decrease in proliferating SGZ precursors that occurred in $p63^{+/-}$ mice (Fig. 6*D*). Similarly, we confirmed the neuronal phenotype by administering BrdU to mice and then assessing BrdU-positive, NeuN-positive neurons in the dentate gyrus 1 month later; p53 ablation resulted in more newborn neurons relative to WTs and completely rescued the decrease in newborn neurons seen in $p63^{+/-}$ mice (Fig. 6*E*).

To ask whether p53 ablation mediated these effects by rescuing the increased cell death that occurred in $p63^{+/-}$ mice, we quantified the proportion of CC3-positive neural precursors and newborn neurons in the dentate gyrus. p53KOs had significantly fewer Sox2-positive, CC3-positive and DCX-positive, CC3-positive cells in the dentate gyrus than did WT mice (Fig. 6*F*,*G*). In contrast, ~25–30% of SGZ precursors and newborn neurons were CC3 positive in $p63^{+/-}$ mice, and this was rescued to WT levels by coincident p53 ablation (Fig. 6*F*,*G*). Similar results were obtained when we performed TUNEL assays; almost 30% of Sox2-positive precursors were TUNEL positive in the $p63^{+/-}$ SGZ, and this was rescued to WT levels with coincident p53 ablation (Fig. 6*H*).

We also examined SVZ precursors in these mice. Initially, we administered BrdU and 1 d later quantified the proportion of proliferating BrdU-positive, Sox2-positive precursors. Coincident p53 ablation rescued the small but significant decrease in proliferating Sox2-positive precursors observed in the $p63^{+/-}$ SVZ (Fig. 6*I*). To ask whether this rescue was attributable to alterations in cell death, we analyzed similar sections by immunostaining for CC3 or by performing TUNEL assays. p63 heterozygosity caused an increase of almost 2.5-fold in the proportion of Sox2-positive SVZ precursors that were apoptotic, and this was rescued back to WT levels by p53 ablation (Fig. 6*J*,*K*). Finally, we quantified adult-born olfactory neurons by administering BrdU and counting BrdU-positive olfactory bulb cells 1 month later. This analysis demonstrated that, as reported previously (Gil-Perotin et al., 2011), p53KOs had increased numbers of newborn olfactory bulb neurons relative to WTs (Fig. 6*L*) and that p53 ablation rescued the decreased numbers of adult-born olfactory neurons seen in the $p63^{+/-}$ mice (Fig. 6*L*). Thus, p63 promotes survival of adult neural precursors and adult-born neurons by inhibiting p53-dependent cell death.

Acute conditional deletion of p63 in adult neural precursors causes deficits in hippocampus-dependent learning

To ask whether this p63 prosurvival activity was functionally important, we characterized aspects of hippocampus-dependent memory formation that are known to require adult neurogenesis. To do this, we acutely ablated p63 in adult neural precursors by treating 1-month-old $p63^{fl/fl}$;*nestin–CreERT2*$^{+/\varnothing}$;*Rosa26R*$^{YFP/YFP}$ mice with tamoxifen as for the neuroanatomy experiments. As controls, we used $p63^{+/+}$;*nestin–CreERT2*$^{+/\varnothing}$;*Rosa26R*$^{YFP/YFP}$ mice. Both groups of mice were treated for three cycles of tamoxifen treatment and, at 4 months of age, were examined for spatial memory formation using the hidden-platform version of the Morris water maze in which mice were trained to find a platform submerged under the pool surface using spatial cues around the room. Specifically, mice were trained for 6 d (two blocks of three trials a day), and spatial memory was evaluated in a series of probe tests (conducted on day 1 and day 4 before training and on day 7 after training was complete) in which the platform was removed from the pool (Fig. 7*A*, top). For each probe test, we quantified the amount of time mice spent searching in the target zone (20 cm radius, centered on the location of the platform during training; 11% of the pool surface) versus the time spent in an average of three other equivalent zones of the pool (Fig. 7*A*, bottom) (de Hoz et al., 2004; Teixeira et al., 2006; Maei et al., 2009). A probe test conducted on day 1 demonstrated that, before training, neither $p63^{fl/fl}$;*nestin–CreERT2*$^{+/\varnothing}$;*Rosa26R*$^{YFP/YFP}$ nor $p63^{+/+}$;*nestin–CreERT2*$^{+/\varnothing}$;*Rosa26R*$^{YFP/YFP}$ mice showed a preference for the target zone versus other zones (Fig. 7*B*,*C*), as expected. On days 4 and 7, the control $p63^{+/+}$;*nestin–CreERT2*$^{+/\varnothing}$;*Rosa26R*$^{YFP/YFP}$ mice showed strong spatial memory, spending more time in the target zone than in other areas of the pool (Fig. 7*B*,*C*). In contrast, spatial memory formation was attenuated in the $p63^{fl/fl}$;*nestin–CreERT2*$^{+/\varnothing}$;*Rosa26R*$^{YFP/YFP}$ mice at both 4 and 7 d (Fig. 7*B*,*C*). An ANOVA comparing time in the target zone only across probe sets showed a genotype × test interaction ($F_{(2,26)} = 5.79$, $p < 0.05$; genotype, $F_{(1,13)} = 4.56$, $p < 0.05$; test, $F_{(2,26)} = 34.44$, $p < 0.001$.) *Post hoc* Newman–Keuls tests performed on this significant interaction demonstrated that the control but not $p63^{fl/fl}$;*nestin–CreERT2*$^{+/\varnothing}$;Ros*a26R*$^{YFP/YFP}$ mice

←

(*Figure legend continued.*) spheres cultured with 50 nM tamoxifen). Spheres were then immunostained for YFP (green, ***A***) and CC3 (red, ***A***), and the proportion of YFP-positive cells that expressed CC3 was quantified (***B***). Control cultures were treated with vehicle alone (0 tamoxifen group in ***B***), and, because none of these cells expressed YFP, the proportion of total CC3-positive cells was determined. *$p < 0.05$, **$p < 0.01$, ***$p < 0.001$; $n = 3$ animals each, analyzed in two independent experiments. Scale bar, 25 μm. ***C***, ***D***, Primary neurosphere numbers in cultures of $p63^{+/+}$ (***C***) or $p63^{fl/fl}$ (***D***) SVZ cells that were dissociated, transduced with 25 M.O.I. EGFP or Cre recombinase-expressing adenovirus (Ad EGFP and Ad Cre) at 3 d and quantified 3 d later. Controls (C) were sister cultures with no adenovirus added. **$p < 0.01$; $n = 3$ $p63^{+/+}$ and $p63^{fl/fl}$ mice; cells from each animal were plated independently, and each condition was performed in triplicate for each animal. Similar results were obtained in additional experiments. ***E***, ***F***, Quantification of primary neurosphere numbers in cultures of TA$p63^{fl/fl}$ (***E***) or ΔN$p63^{fl/fl}$ (***F***) SVZ cells transduced with EGFP or Cre adenovirus as in ***C*** and ***D***. Numbers were normalized to the EGFP-transduced cultures as 100%. For ***E***, $p = 0.19$, $n = 5$ TA$p63^{fl/fl}$ mice; for ***F***, ***$p < 0.001$, $n = 7$ ΔN$p63^{fl/fl}$ mice; in both experiments, cells from each animal were plated independently, and each conditioned was performed in triplicate for each animal. ***G***, Primary neurosphere numbers in cultures of ΔN$p63^{fl/fl}$ SVZ cells transduced at 3 d with EGFP or Cre adenoviruses, treated with ZVAD or vehicle (DMSO) after 1 d, and quantified 3 d later. Numbers were normalized to EGFP-transduced cultures treated with vehicle as 100%. ANOVA, $F_{(3,8)} = 9.59$; **$p = 0.005$, $n = 3$ mice, cells from each animal plated independently, and each condition performed in triplicate for each animal. Similar results were obtained in additional experiments. ***H***, RT-PCR analysis of equal amounts of total RNA isolated from WT SVZ neurospheres that were transduced with scrambled, p53, or PUMA shRNA lentiviruses on day 2 and analyzed for p53, p63, p73, PUMA, and GADPH mRNAs on day 6. ***I***, Primary neurosphere numbers in cultures of ΔN$p63^{fl/fl}$ SVZ cells transduced with lentiviruses expressing p53 or scrambled (Scr) shRNAs on day 2 and then again with EGFP or Cre-expressing lentivirus on day 4. Numbers were quantified on day 6. ANOVA, $F_{(3,28)} = 15.18$; ***$p < 0.001$, $n = 8$ mice, 4 each in two independent experiments. Cells from each animal were plated independently, and each condition was performed in triplicate. ***J***, Quantitative real-time PCR for PUMA mRNA in total RNA isolated from $p63^{+/-}$ and WT SVZ neurospheres. *$p < 0.05$; $n = 4$ mice per group, analyzed in two independent experiments. ***K***, Primary neurosphere numbers in cultures of $p63^{fl/fl}$ SVZ cells transduced with lentivirus expressing PUMA or scrambled (Scr) shRNAs on day 2 and then again with EGFP or Cre-expressing lentivirus on day 4. ANOVA, $F_{(3,28)} = 15.18$; ***$p < 0.001$, $n = 8$ mice, analyzed in two independent experiments. Cells from each animal were plated independently, and each condition was performed in triplicate. In all panels, error bars denote SEM.

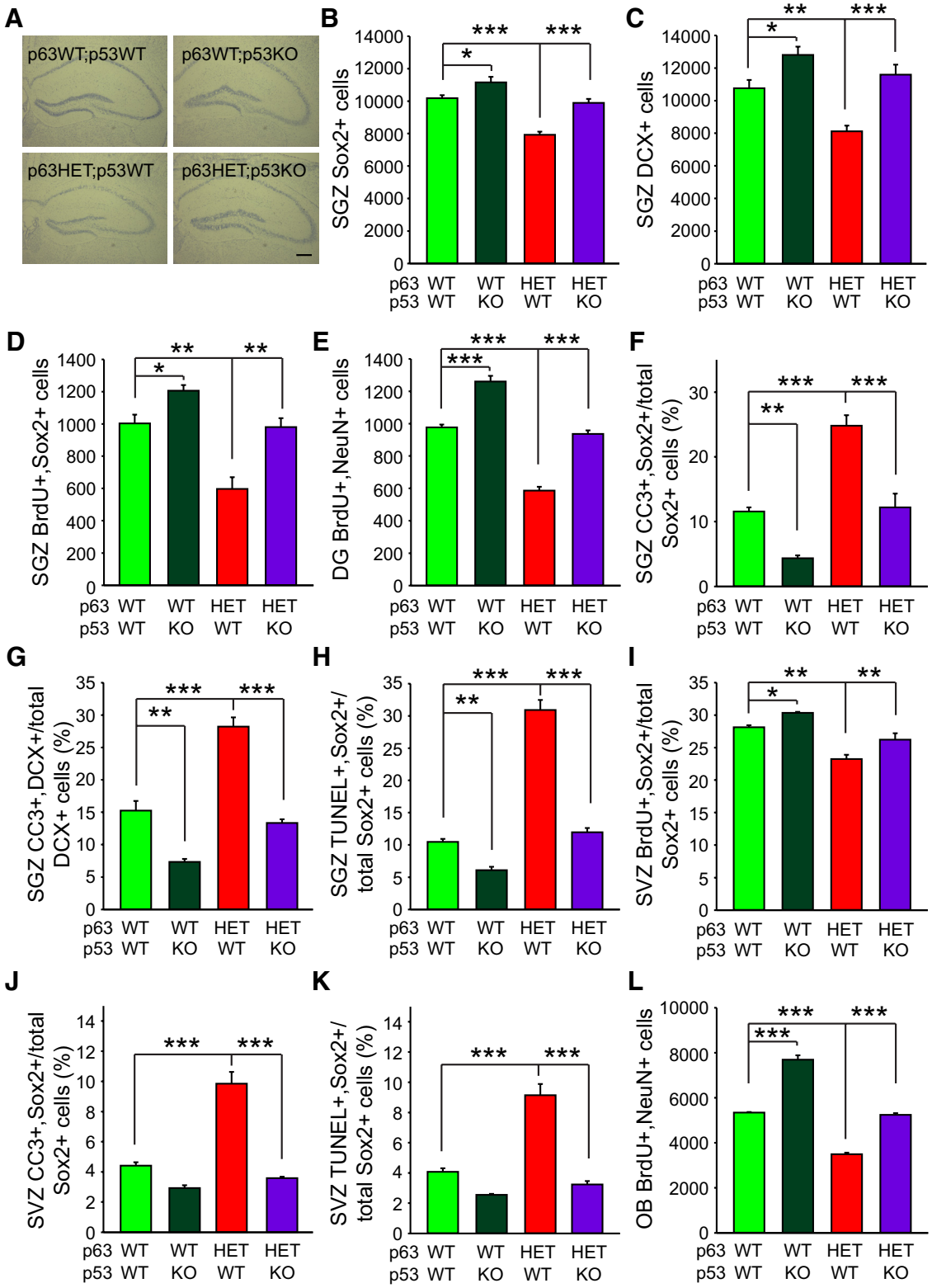

Figure 6. The $p63^{+/-}$ deficit in NPCs and adult-born neurons in 3-month-old mice is rescued by coincident ablation of p53 *in vivo*. Coronal sections at the level of the hippocampus (***A–H***), lateral ventricles (***I–K***), and olfactory bulb (***L***) of 3-month-old $p63^{+/+}$;$p53^{+/+}$ (p63WT;p53WT), $p63^{+/+}$;$p53^{-/-}$ (p63WT;p53KO), $p63^{+/-}$;$p53^{+/+}$ (p63HET;p53WT), and $p63^{+/-}$;$p53^{-/-}$ (p63HET; p53KO) mice were analyzed for precursor and newborn neuron phenotypes, and quantification was performed as in Figures 2 and 3. ***A***, Representative micrographs of coronal, Nissl-stained sections at the level of the hippocampus. Scale bar, 250 μm. ***B***, ***C***, Quantification of the total number of Sox2-positive precursors (***B***) and DCX-positive newborn neurons (***C***) in the SGZ. For ***B***: ANOVA, $F_{(3,12)} = 30.78$; ***$p < 0.001$, $n = 4$ animals per group. For ***C***: ANOVA, $F_{(3,12)} = 15.64$; ***$p < 0.001$, $n = 4$ animals per group. ***D***, Quantification of the total number of BrdU-positive, Sox2-positive SGZ cells 1 d after BrdU injection. ANOVA, $F_{(3,8)} = 20.91$; ***$p < 0.001$, $n = 3$ animals per group. ***E***, Quantification of the total number of BrdU-positive, NeuN-positive neurons in the dentate gyrus 30 d after BrdU injection. ANOVA, $F_{(3,8)} = 115.7$; ***$p < 0.001$, $n = 3$ animals per group. ***F***, ***G***, Quantification of the proportion of Sox2-positive (***F***) or DCX-positive (***G***) dentate gyrus cells that are also positive for CC3. For ***F***: ANOVA, $F_{(3,8)} = 37.11$; ***$p < 0.001$, $n = 3$ animals per group; 90–242 total double-positive cells were counted per hippocampus. For ***G***: ANOVA, $F_{(3,8)} = 64.23$; ***$p < 0.001$, $n = 3$ animals per group, 92–250 total double-positive cells were counted per hippocampus. ***H***, Quantification of the proportion of Sox2-positive cells in the (*Figure legend continues.*)

showed evidence of spatial memory formation in the day 4 probe and that, even on day 7, $p63^{fl/fl}$;*nestin–CreERT2*$^{+/\varnothing}$;$Rosa26R^{YFP/YFP}$ mice only showed weak spatial memory. In contrast to these deficits in spatial memory, $p63^{fl/fl}$ mice demonstrated normal swim speed over training ($p > 0.05$) and were not different from their control littermates in a visible (cued) version of the water maze (ANOVA; genotype, $F_{(1,16)} = 0.02$, $p > 0.05$; training day, $F_{(1,16)} = 14.48$, $p < 0.01$; $n = 8$, $p63^{+/+}$;*nestin–CreERT2*$^{+/\varnothing}$;$Rosa26R^{YFP/YFP}$; $n = 10$, $p63^{fl/fl}$;*nestin–CreERT2*$^{+/\varnothing}$;$Rosa26R^{YFP/YFP}$). Thus, the deficit in spatial memory formation could not be attributed to nonspecific performance variables.

To confirm that the acute loss of p63 in adult precursors caused deficits in hippocampus-dependent learning, we also performed a standard delay context fear memory task (Kim and Fanselow, 1992; Nakashiba et al., 2012). Results of this task demonstrated that $p63^{fl/fl}$;*nestin–CreERT2*$^{+/\varnothing}$;$Rosa26R^{YFP/YFP}$ mice had deficits in context fear memory relative to the control $p63^{+/+}$;*nestin–CreERT2*$^{+/\varnothing}$;$Rosa26R^{YFP/YFP}$ mice (Fig. 7*D*). We then used a context preexposure task, a version of context fear that is critically dependent on the hippocampus (Matus-Amat et al., 2004; Rudy et al., 2004). Unlike traditional context fear conditioning experiments, the context preexposure task temporally separates the context acquisition phase of the experiment from the association of the context with the shock. In this task, rodents are exposed to the context for 10 min (without shock) and, the following day, receive an immediate shock after being replaced in the context; only animals that were preexposed to the context show high levels of freezing when subsequently tested (Kiernan and Westbrook, 1993). As predicted for this task, both $p63^{+/+}$;*nestin–CreERT2*$^{+/\varnothing}$;$Rosa26R^{YFP/YFP}$ and $p63^{fl/fl}$;*nestin–CreERT2*$^{+/\varnothing}$;$Rosa26R^{YFP/YFP}$ mice that were not preexposed (NPE) to the context the day before receiving an immediate footshock after context placement showed low freezing when subsequently tested (Fig. 7*E*). As expected, the control $p63^{+/+}$;*nestin–CreERT2*$^{+/\varnothing}$;$Rosa26R^{YFP/YFP}$ that were preexposed (PE) to the context showed higher freezing than either group of NPE mice (Fig. 7*E*), which both displayed equally low freezing, as shown by *post hoc* Newman–Keuls tests. However, the PE $p63^{fl/fl}$;*nestin–CreERT2*$^{+/\varnothing}$;$Rosa26R^{YFP/YFP}$ mice froze significantly less than did the PE $p63^{+/+}$;*nestin–CreERT2*$^{+/\varnothing}$;$Rosa26R^{YFP/YFP}$ mice (Fig. 7*E*). In contrast, both groups showed normal distance traveled and anxiety behaviors in the open field (Fig. 7*F*,*G*), making it unlikely that the spatial and contextual memory deficits are attributable to nonspecific impairments in motor function or increases in anxiety. Thus, inducible ablation of p63 in adult neural precursors and their adult-born neuronal progeny is sufficient to cause deficits in hippocampus-dependent learning.

Similar behavioral deficits were observed in 3-month-old $p63^{+/-}$ mice relative to their WT littermates, confirming the data obtained with the $p63^{fl/fl}$;*nestin–CreERT2*$^{+/\varnothing}$;$Rosa26R^{YFP/YFP}$ mice. With regard to the water maze, analysis of the probe tests showed that, as expected, on day 1, before training began, neither $p63^{+/+}$ or $p63^{+/-}$ mice showed a preference for the target zone over an average of the other zones (Fig. 7*H*,*I*). On day 4, $p63^{+/+}$ mice showed spatial memory, spending more time in the target versus other zones, whereas $p63^{+/-}$ mice did not and spent equivalent amounts of time in the target and other zones (Fig. 7*H*,*I*). $p63^{+/-}$ mice did exhibit evidence of weak spatial memory after all training was complete on day 7, but they continued to show a deficit in spatial memory relative to their WT littermates, spending less time in the target zone than $p63^{+/+}$ mice (Fig. 7*H*,*I*). A comparison of the time spent in the target zone only across probe tests confirmed that, although $p63^{+/+}$ mice showed robust spatial memory formation on day 4, $p63^{+/-}$ mice did not show evidence of spatial memory until day 7 (two-way ANOVA and *post hoc* Newman–Keuls test; genotype × test interaction, $F_{(2,36)} = 4.69$, $p < 0.05$; genotype, $F_{(1,18)} = 16.22$, $p < 0.001$; test, $F_{(2,36)} = 19.98$, $p < 0.001$).

Similarly, $p63^{+/-}$ mice showed a deficit relative to $p63^{+/+}$ mice in both the standard test of context fear memory (Fig. 7*J*) and in the context preexposure fear memory task (Fig. 7*K*). With regard to the latter, both $p63^{+/+}$ and $p63^{+/-}$ mice that were not preexposed (NPE) to the context showed low freezing when subsequently tested, and WT $p63^{+/+}$ mice that were preexposed (PE) to the context showed robust freezing when tested (Fig. 7*K*). In contrast, $p63^{+/-}$ mice that were preexposed to the context showed a deficit in freezing when later tested (Fig. 7*K*). These deficits were not attributable to nonspecific impairments because $p63^{+/-}$ mice showed normal distance traveled and anxiety behavior in the open field (Fig. 7*L*,*M*).

Discussion

The molecular mechanisms ensuring the survival of adult NPCs and newborn neurons and the potential relevance of these mechanisms to cognitive function are poorly understood. Here we show that p63 is a key determinant of NPC survival. Depletion of p63, either conditionally in adult NPCs or by haploinsufficiency, caused death of both precursors and adult-born neurons and ultimately led to cognitive deficits. Our culture experiments indicate that these phenotypes were attributable to the loss of ΔNp63, which promotes neural precursor survival at least in part by silencing a p53–PUMA-dependent death pathway. Moreover, coincident ablation of p53 *in vivo* was sufficient to rescue the enhanced apoptosis and decreased neurogenesis that occurs in $p63^{+/-}$ mice. Thus, p63 plays a critical role in maintaining normal numbers of adult NPCs and adult-born neurons, thereby regulating hippocampal-dependent memory formation.

We and others have observed that the basal rate of adult NPC apoptosis is ~8–15% (Bunk et al., 2010; Malone et al., 2012; Sun et al., 2012), and we therefore hypothesized that any increase in this basal rate of apoptosis would result in decreased NPC pools, decreased adult neurogenesis, and subsequent cognitive impairments. Indeed, decreasing the levels of p63 in the $p63^{+/-}$ mouse or by conditional ablation of p63 in NPCs resulted in a doubling of the number of CC3 or TUNEL-positive NPCs and newborn neurons and a 30–40% reduction in new neurons that integrated in the SGZ and olfactory bulb. Therefore, we conclude that maintaining the basal rate of NPC survival is important to sustain neurogenesis in the adult mouse and that any alterations that might affect this survival, even in a small way, will likely have significant consequences behaviorally.

How does ΔNp63 suppress apoptosis in NPCs? One way it might do so is by inhibiting the apoptotic actions of p53. In this

←

(*Figure legend continued.*) dentate gyrus that were also positive for TUNEL. ANOVA, $F_{(3,8)} = 142.9$; ***$p < 0.001$, $n = 3$ animals per group, 104–250 total double-positive cells were counted per hippocampus. ***I***, Quantification of the proportion of Sox2-positive cells within the SVZ that were also positive for BrdU 1 d after BrdU injection. ANOVA, $F_{(3,8)} = 24.28$; ***$p < 0.001$, $n = 3$ animals per group. ***J***, ***K***, Quantification of the proportion of Sox2-positive SVZ cells that were also positive for CC3 (***J***) or TUNEL (***K***). For ***J***: ANOVA, $F_{(3,8)} = 56.47$; ***$p < 0.001$, $n = 3$ animals per group, 133–316 total double-positive cells were counted per SVZ. For ***K***: ANOVA, $F_{(3,8)} = 54.52$; ***$p < 0.001$, $n = 3$ animals per group, 122–280 total double-positive cells were counted per SVZ. ***L***, Quantification of the total number of BrdU-positive, NeuN-positive neurons in the olfactory bulb 30 d after BrdU injection. ANOVA, $F_{(3,8)} = 260.3$; ***$p < 0.001$, $n = 3$ animals per group. In all panels, error bars denote SEM.

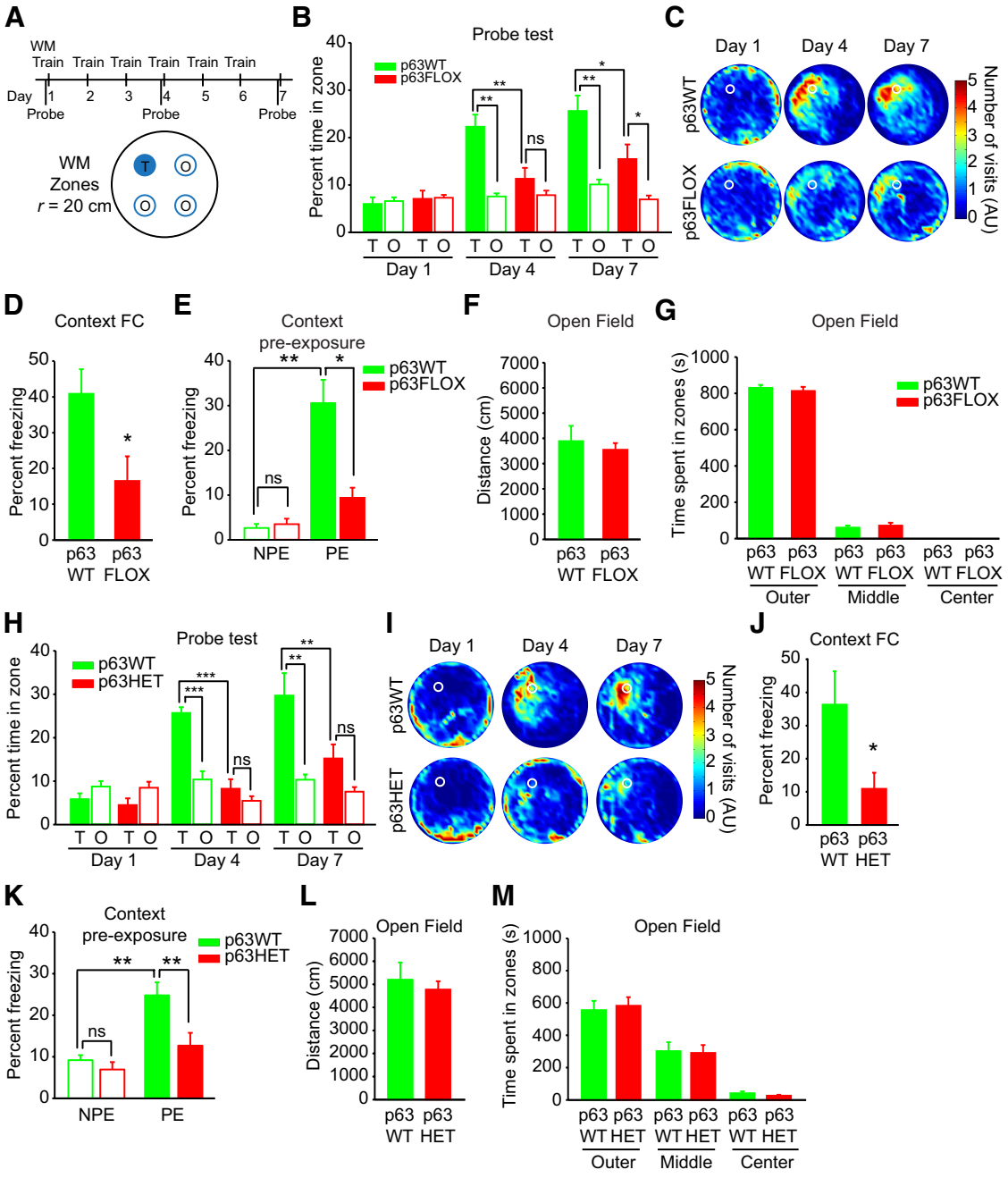

Figure 7. Acute ablation of p63 in adult neural precursors impairs hippocampus-dependent learning. ***A–G***, Four-month-old *p63*$^{+/+}$;*nestin–CreERT2*$^{+/Ø}$;*Rosa26R*$^{YFP/YFP}$ (p63WT) and *p63*$^{fl/fl}$;*nestin–CreERT2*$^{+/Ø}$;*Rosa26R*$^{YFP/YFP}$ (p63FLOX) mice were trained in the hidden-platform version of the Morris water maze (WM). ***A***, To assess spatial memory formation, probe tests were conducted on days 1 and 4 before training and on day 7 (after training was completed). During the probe test, the platform was removed from the pool and the amount of time mice spent in the target (T) zone (in which the platform was located during training) was compared with the average time spent in the equally sized other (O) zones. ***B***, Quantitative analysis of the time spent in the target zone (Target) versus equivalent zones in the other three quadrants (Other). Two-way ANOVA; day 1, genotype × zone, $F_{(1,13)} = 0.01$, $p > 0.05$; genotype, $F_{(1,18)} = 0.61$, $p > 0.05$; zone, $F_{(1,18)} = 0.09$, $p > 0.05$; day 4, genotype × zone, $F_{(1,13)} = 7.04$, $p < 0.05$; genotype, $F_{(1,13)} = 12.82$, $p < 0.01$; zone, $F_{(1,13)} = 18.44$, $p < 0.001$; day 7, genotype × Zone, $F_{(1,13)} = 0.84$, $p > 0.05$; genotype, $F_{(1,13)} = 8.41$, $p < 0.05$; zone, $F_{(1,13)} = 23.03$, $p < 0.001$; $n = 8$ p63WT, 7 p63FLOX. ***C***, Density plots of grouped data showing where in the pool the p63WT and p63FLOX mice concentrated their searches during probe tests on days 1, 4, and 7. Color scale represents the number of visits per animal per 5 × 5 cm area of the pool. During training, the platform was located in top left of pool (white circle). AU, Arbitrary units. ***D***, Percentage of time spent freezing in the standard delay context fear memory task for *p63*$^{+/+}$;*nestin–CreERT2*$^{+/Ø}$;*Rosa26R*$^{YFP/YFP}$ (p63WT) and *p63*$^{fl/fl}$;*nestin–CreERT2*$^{+/Ø}$;*Rosa26R*$^{YFP/YFP}$ (p63FLOX) mice. ANOVA, $F_{(1,15)} = 6.23$, $^{*}p < 0.05$, $n = 11$ p63WT and 6 p63FLOX. ***E***, *p63*$^{+/+}$;*nestin–CreERT2*$^{+/Ø}$;*Rosa26R*$^{YFP/YFP}$ (p63WT) and *p63*$^{fl/fl}$;*nestin–CreERT2*$^{+/Ø}$;*Rosa26R*$^{YFP/YFP}$ (p63FLOX) mice were tested in the context preexposure task, comparing groups of mice that were preexposed (PE) or non-preexposed (NPE) to the context the day before receiving a shock. ANOVA, $F_{(3,33)} = 9.56$, $p < 0.001$; $^{*}p < 0.05$; $^{**}p < 0.01$; $n = 9$ NPE p63WT, 9 PE p63WT, 9 NPE p63FLOX, and 8 PE p63FLOX. ***F,G***, Open-field analysis for *p63*$^{+/+}$;*nestin–CreERT2*$^{+/Ø}$;*Rosa26R*$^{YFP/YFP}$ (p63WT) and *p63*$^{fl/fl}$;*nestin–CreERT2*$^{+/Ø}$;*Rosa26R*$^{YFP/YFP}$ (p63FLOX) mice showing the distance traveled (***F***, in centimeters) and time spent in the outer, middle, and center regions (***G***, in seconds) in the open field. ANOVA, $p > 0.05$; $n = 8$ p63WT and 7 p63FLOX. In all panels, error bars denote SEM. ***H–M***, Three-month-old *p63*$^{+/+}$ (p63WT) and *p63*$^{+/-}$ (p63HET) mice were trained in the hidden-platform version of the Morris water maze. ***H***, Percentage of time spent in the target zone (T) versus equivalent zones in the other three quadrants (O) in probe tests conducted on days 1, 4, and 7. Two-way ANOVA, day 1, genotype × zone interaction, $F_{(1,18)} = 0.11$, $p > 0.05$ or main effect of genotype, $F_{(1,18)} = 0.52$, $p > 0.05$; zone, $F_{(1,18)} = 4.55$, $p < 0.05$; day 4, genotype × zone, $F_{(1,18)} = 46.80$, $p < 0.001$; genotype, $F_{(1,18)} = 36.70$, $p < 0.001$; zone, $F_{(1,18)} = 82.26$, $p < 0.001$; day 7, genotype × zone, $F_{(1,18)} = 1.85$, $p > 0.05$; genotype, $F_{(1,18)} = 8.26$, $p < 0.05$; zone, $F_{(1,18)} = 14.96$, $p < 0.001$; $^{**}p < 0.01$, $^{***}p < 0.001$, NS = $p > 0.05$; $n = 10$ per group. ***I***, Density plots for grouped data showing where the p63WT and p63HET mice concentrated their searches during probe tests on days 1, 4, and 7. Color scale represents the number of visits per animal per 5 × 5 cm area of the pool. During training, (*Figure legend continues.*)

regard, we show that knockdown of p53 in neurospheres rescued the increased apoptosis caused by conditional p63 ablation. Likewise, knock-out of p53 *in vivo* rescued the enhanced apoptosis of NPCs and newly born neurons observed in $p63^{+/-}$ mice. In this regard, deletion of p53 has been shown previously to increase the survival of SVZ-derived neurospheres (Meletis et al., 2006), and, when p53 is constitutively activated in mice by a knock-in mutation, this depletes SGZ precursors in a manner dependent on the p53 apoptotic effector PUMA (Liu et al., 2010). Our results confirm and extend these previous studies; we show an increase in adult NPCs and adult-born neurons in $p53^{-/-}$ mice, enhanced levels of PUMA in $p63^{+/-}$ neurospheres, and a rescue of the survival of neurospheres depleted of ΔNp63 by suppressing either p53 or PUMA. Thus, although ΔNp63 can suppress apoptosis in a number of ways (Yang and McKeon, 2000), our data support a model in which p53 is a major ΔNp63 pro-apoptotic target in NPCs, with ΔNp63 directly inhibiting p53 function by either directly competing for p53 target promoters and/or binding to and sequestering p53 by forming inactive tetramers (Yang and McKeon, 2000). An alternative mechanism is that ΔNp63 might prevent premature cell cycle exit of NPCs, one of the proposed roles for this gene in epithelial cells (Koster et al., 2005). In keratinocytes, ΔNp63 regulates the cell cycle through its direct or indirect transcriptional suppression of the cell cycle inhibitors $p21^{WAF1}$ and $p16^{INK4a}$ (Westfall et al., 2003; Keyes et al., 2005). However, the consequence of elevated $p21^{WAF1}$ and $p16^{INK4a}$ after p63 knockdown or ablation was premature senescence (Westfall et al., 2003; Keyes et al., 2005) rather than apoptosis as we observe here.

We previously reported roles for TAp73 in embryonic and adult NPCs and for TAp63 in neural crest-like dermal stem cells (Su et al., 2009; Fujitani et al., 2010). In both cases, the TA isoforms regulated self-renewal by inhibiting precursor differentiation or cell cycle arrest. We have also shown that ΔNp63, when depleted by *in utero* electroporation in NPCs, caused an enhancement of embryonic cortical precursor apoptosis (Dugani et al., 2009). However, Holembowski et al. (2011) examined the p63 knock-out embryonic cortex and concluded that there was no difference in embryonic forebrain NPC development. In contrast, we show here that, in the adult brain, heterozygosity or acute ablation of p63 results in a 30–40% loss in SVZ and SGZ NPCs and associated neurogenesis and ultimately causes deficits in NPC-related hippocampus-dependent cognition.

At the molecular level, both intrinsic and extrinsic cues have been described as adult neurogenesis modulators, including Sox2 and TLX (Trophoblast leukocyte common antigen) in NPC self-renewal, FGF and EGF receptors in NPC proliferation, and Wnt and VEGF in NPC differentiation (Ming and Song, 2011). However, little is known about the genes regulating adult NPC survival and how this might affect NPC-dependent learning. Results presented here identifying a prosurvival protein, p63, as an important regulator of adult neurogenesis indicate that cell survival is one key regulatory point in this regard. Moreover, because p63 is also expressed in human cortex and hippocampus (Hernández-Acosta et al., 2011), then our results raise the possibility that p63 might regulate human hippocampal neurogenesis, something that could be relevant for humans with p63 mutations (Brunner et al., 2002).

Here we show that conditional ablation of p63 in adult NPCs and adult-born neurons causes deficits in the numbers of these two cell types coincident with impaired memory on the hidden-platform version of the water maze and two versions of context fear conditioning. This behavioral profile of specific hippocampal memory formation impairment was remarkably consistent with that seen in mice in which p63 is haploinsufficient. The finding that disrupting adult-born neurons induces a deficit in hippocampal-dependent memory is in agreement with many previous findings. For instance, several studies report deficits in contextual fear conditioning (Saxe et al., 2006; Imayoshi et al., 2008) and spatial memory formation assessed in the water maze (Dupret et al., 2008; Deng et al., 2009; Garthe et al., 2009) after ablation of adult neurogenesis. Additionally, decreased hippocampal neurogenesis resulting from genetic deletion of the orphan receptor TLX (Ming and Song, 2011) or the fragile X syndrome protein FMRP (Guo et al., 2011) also led to impairments in the water maze and radial arm maze, respectively.

Our findings showing that p63 is a key prosurvival protein for neural precursors add to a growing body of literature indicating an important role for the p53 family in adult NPCs. With regard to p73, four groups showed that p73 was critical for the self-renewal of NPCs in the embryonic and adult brain and that TAp73 was the isoform responsible for normal hippocampal formation, adult neurogenesis, and self-renewal of NPCs (Fujitani et al., 2010; Talos et al., 2010; Flores, 2011). As for p53, it regulates the number of NPCs in the adult brain by regulating both survival and proliferation (Meletis et al., 2006; Gil-Perotin et al., 2011). Thus, the three p53 family members (p53, p63, and p73) play distinct roles in the maintenance of adult NPC pools. p53 negatively inhibits self-renewal, proliferation, and survival, whereas ΔNp63 counteracts the pro-apoptotic activity of p53. TAp73 maintains NPC pools by inhibiting inappropriate neurogenesis, in part by transcriptionally activating the HEY2 neurogenesis suppressor (Fujitani et al., 2010) and possibly by enhancing the expression of self-renewal regulators such as Sox2 (Talos et al., 2010). Perturbations in the expression or activity of any of these family members will ultimately alter the size of the NPC pool, with significant repercussions for cognitive function.

←

(*Figure legend continued.*) the platform was located in top left of pool (white circle). AU, Arbitrary units. ***J***, Percentage of time spent freezing in the standard delay context fear memory task for $p63^{+/+}$ (p63WT) and $p63^{+/-}$ (p63HET) mice. ANOVA, $F_{(1,6)} = 8.03$, $^{*}p < 0.05$, $n =$ 4 per group. ***K***, $p63^{+/+}$ (p63WT) and $p63^{+/-}$ (p63HET) mice were tested in the context preexposure task comparing groups of mice that were preexposed (PE) or non-preexposed (NPE) to the context the day before receiving a shock. ANOVA, $F_{(3,33)} = 9.57$, $^{**}p < 0.001$; $n =$ 7 NPE $p63^{+/+}$, 12 PE $p63^{+/+}$, 9 NPE $p63^{+/-}$, and 9 PE $p63^{+/-}$. ***L***, ***M***, Open-field analysis for $p63^{+/+}$ (p63WT) and $p63^{+/-}$ (p63HET) mice, showing the distance traveled (***L***, in centimeters) and time spent in the outer, middle, and center regions (***M***, in seconds) in the open field. ANOVA, $p > 0.05$; $n = 4$ per group. In all panels, error bars denote SEM.

References

Arruda-Carvalho M, Sakaguchi M, Akers KG, Josselyn SA, Frankland PW (2011) Posttraining ablation of adult-generated neurons degrades previously acquired memories. J Neurosci 31:15113–15127. CrossRef Medline

Biernaskie JA, McKenzie IA, Toma JG, Miller FD (2006) Isolation of skin-derived precursors (SKPs) and differentiation and enrichment of their Schwann cell progeny. Nat Protoc 1:2803–2812. CrossRef Medline

Brunner HG, Hamel BC, Van Bokhoven H (2002) The p63 gene in EEC and other syndromes. J Med Genet 39:377–381. CrossRef Medline

Bunk EC, König HG, Bernas T, Engel T, Henshall DC, Kirby BP, Prehn JH (2010) BH3-only proteins BIM and PUMA in the regulation of survival and neuronal differentiation of newly generated cells in the adult mouse hippocampus. Cell Death Dis 1:e15. CrossRef Medline

Cancino GI, Toledo EM, Leal NR, Hernandez DE, Yévenes LF, Inestrosa NC, Alvarez AR (2008) STI571 prevents apoptosis, tau phosphorylation and behavioural impairments induced by Alzheimer's beta-amyloid deposits. Brain 131:2425–2442. CrossRef Medline

Cancino GI, Miller FD, Kaplan DR (2013) p73 haploinsufficiency causes tau

hyperphosphorylation and tau kinase dysregulation in mouse models of aging and Alzheimer's disease. Neurobiol Aging 34:387–399. CrossRef Medline

de Hoz L, Martin SJ, Morris RG (2004) Forgetting, reminding, and remembering: the retrieval of lost spatial memory. PLoS Biol 2:E225. CrossRef Medline

Deng W, Saxe MD, Gallina IS, Gage FH (2009) Adult-born hippocampal dentate granule cells undergoing maturation modulate learning and memory in the brain. J Neurosci 29:13532–13542. CrossRef Medline

Deng W, Aimone JB, Gage FH (2010) New neurons and new memories: how does adult hippocampal neurogenesis affect learning and memory? Nat Rev Neurosci 11:339–350. CrossRef Medline

Dötsch V, Bernassola F, Coutandin D, Candi E, Melino G (2010) p63 and p73, the ancestors of p53. Cold Spring Harb Perspect Biol 2:a004887. CrossRef Medline

Dugani CB, Paquin A, Fujitani M, Kaplan DR, Miller FD (2009) p63 antagonizes p53 to promote the survival of embryonic neural precursor cells. J Neurosci 29:6710–6721. CrossRef Medline

Dupret D, Revest JM, Koehl M, Ichas F, De Giorgi F, Costet P, Abrous DN, Piazza PV (2008) Spatial relational memory requires hippocampal adult neurogenesis. PLoS One 3:e1959. CrossRef Medline

Flores ER (2011) p73 is critical for the persistence of memory. Cell Death Differ 18:381–382. CrossRef Medline

Frankland PW, Josselyn SA, Anagnostaras SG, Kogan JH, Takahashi E, Silva AJ (2004) Consolidation of CS and US representations in associative fear conditioning. Hippocampus 14:557–569. CrossRef Medline

Fujitani M, Cancino GI, Dugani CB, Weaver IC, Gauthier-Fisher A, Paquin A, Mak TW, Wojtowicz MJ, Miller FD, Kaplan DR (2010) TAp73 acts via the bHLH Hey2 to promote long-term maintenance of neural precursors. Curr Biol 20:2058–2065. CrossRef Medline

Garthe A, Behr J, Kempermann G (2009) Adult-generated hippocampal neurons allow the flexible use of spatially precise learning strategies. PLoS One 4:e5464. CrossRef Medline

Gil-Perotin S, Haines JD, Kaur J, Marin-Husstege M, Spinetta MJ, Kim KH, Duran-Moreno M, Schallert T, Zindy F, Roussel MF, Garcia-Verdugo JM, Casaccia P (2011) Roles of p53 and p27(Kip1) in the regulation of neurogenesis in the murine adult subventricular zone. Eur J Neurosci 34:1040–1052. CrossRef Medline

Guo W, Allan AM, Zong R, Zhang L, Johnson EB, Schaller EG, Murthy AC, Goggin SL, Eisch AJ, Oostra BA, Nelson DL, Jin P, Zhao X (2011) Ablation of Fmrp in adult neural stem cells disrupts hippocampus-dependent learning. Nat Med 17:559–565. CrossRef Medline

Hernández-Acosta NC, Cabrera-Socorro A, Morlans MP, Delgado FJ, Suárez-Solá ML, Sottocornola R, Lu X, González-Gómez M, Meyer G (2011) Dynamic expression of the p53 family members p63 and p73 in the mouse and human telencephalon during development and in adulthood. Brain Res 1372:29–40. CrossRef Medline

Holembowski L, Schulz R, Talos F, Scheel A, Wolff S, Dobbelstein M, Moll U (2011) While p73 is essential, p63 is completely dispensable for the development of the central nervous system. Cell Cycle 10:680–689. CrossRef Medline

Imayoshi I, Sakamoto M, Ohtsuka T, Takao K, Miyakawa T, Yamaguchi M, Mori K, Ikeda T, Itohara S, Kageyama R (2008) Roles of continuous neurogenesis in the structural and functional integrity of the adult forebrain. Nat Neurosci 11:1153–1161. CrossRef Medline

Jacks T, Remington L, Williams BO, Schmitt EM, Halachmi S, Bronson RT, Weinberg RA (1994) Tumor spectrum analysis in p53-mutant mice. Curr Biol 4:1–7. CrossRef Medline

Keyes WM, Wu Y, Vogel H, Guo X, Lowe SW, Mills AA (2005) p63 deficiency activates a program of cellular senescence and leads to accelerated aging. Genes Dev 19:1986–1999. CrossRef Medline

Kiernan MJ, Westbrook RF (1993) Effects of exposure to a to-be-shocked environment upon the rat's freezing response: evidence for facilitation, latent inhibition, and perceptual learning. Q J Exp Psychol B 46:271–288. Medline

Kim JJ, Fanselow MS (1992) Modality-specific retrograde amnesia of fear. Science 256:675–677. CrossRef Medline

Koster MI, Kim S, Roop DR (2005) p63 deficiency: a failure of lineage commitment or stem cell maintenance? J Investig Dermatol Symp Proc 10:118–123. CrossRef Medline

Lagace DC, Whitman MC, Noonan MA, Ables JL, DeCarolis NA, Arguello AA, Donovan MH, Fischer SJ, Farnbauch LA, Beech RD, DiLeone RJ, Greer CA, Mandyam CD, Eisch AJ (2007) Dynamic contribution of nestin-expressing stem cells to adult neurogenesis. J Neurosci 27:12623–12629. CrossRef Medline

Liu D, Ou L, Clemenson GD Jr, Chao C, Lutske ME, Zambetti GP, Gage FH, Xu Y (2010) Puma is required for p53-induced depletion of adult stem cells. Nat Cell Biol 12:993–998. CrossRef Medline

Maei HR, Zaslavsky K, Teixeira CM, Frankland PW (2009) What is the most sensitive measure of water maze probe test performance? Front Integr Neurosci 3:4. CrossRef Medline

Malone CD, Hasan SM, Roome RB, Xiong J, Furlong M, Opferman JT, Vanderluit JL (2012) Mcl-1 regulates the survival of adult neural precursor cells. Mol Cell Neurosci 49:439–447. CrossRef Medline

Matus-Amat P, Higgins EA, Barrientos RM, Rudy JW (2004) The role of the dorsal hippocampus in the acquisition and retrieval of context memory representations. J Neurosci 24:2431–2439. CrossRef Medline

Meletis K, Wirta V, Hede SM, Nistér M, Lundeberg J, Frisén J (2006) p53 suppresses the self-renewal of adult neural stem cells. Development 133:363–369. CrossRef Medline

Mills AA, Zheng B, Wang XJ, Vogel H, Roop DR, Bradley A (1999) p63 is a p53 homologue required for limb and epidermal morphogenesis. Nature 398:708–713. CrossRef Medline

Mills AA, Qi Y, Bradley A (2002) Conditional inactivation of p63 by Cre-mediated excision. Genesis 32:138–141. CrossRef Medline

Ming GL, Song H (2011) Adult neurogenesis in the mammalian brain: significant answers and significant questions. Neuron 70:687–702. CrossRef Medline

Moser E, Moser MB, Andersen P (1993) Spatial learning impairment parallels the magnitude of dorsal hippocampal lesions, but is hardly present following ventral lesions. J Neurosci 13:3916–3925. Medline

Moser MB, Moser EI (1998) Distributed encoding and retrieval of spatial memory in the hippocampus. J Neurosci 18:7535–7542. Medline

Nakashiba T, Cushman JD, Pelkey KA, Renaudineau S, Buhl DL, McHugh TJ, Rodriguez Barrera V, Chittajallu R, Iwamoto KS, McBain CJ, Fanselow MS, Tonegawa S (2012) Young dentate granule cells mediate pattern separation, whereas old granule cells facilitate pattern completion. Cell 149:188–201. CrossRef Medline

Pozniak CD, Barnabé-Heider F, Rymar VV, Lee AF, Sadikot AF, Miller FD (2002) p73 is required for survival and maintenance of CNS neurons. J Neurosci 22:9800–9809. Medline

Rudy JW, Huff NC, Matus-Amat P (2004) Understanding contextual fear conditioning: insights from a two-process model. Neurosci Biobehav Rev 28:675–685. CrossRef Medline

Saxe MD, Battaglia F, Wang JW, Malleret G, David DJ, Monckton JE, Garcia AD, Sofroniew MV, Kandel ER, Santarelli L, Hen R, Drew MR (2006) Ablation of hippocampal neurogenesis impairs contextual fear conditioning and synaptic plasticity in the dentate gyrus. Proc Natl Acad Sci U S A 103:17501–17506. CrossRef Medline

Su X, Paris M, Gi YJ, Tsai KY, Cho MS, Lin YL, Biernaskie JA, Sinha S, Prives C, Pevny LH, Miller FD, Flores ER (2009) TAp63 prevents premature aging by promoting adult stem cell maintenance. Cell Stem Cell 5:64–75. CrossRef Medline

Sun Y, Zhang Y, Wang X, Blomgren K, Zhu C (2012) Apoptosis-inducing factor downregulation increased neuronal progenitor, but not stem cell, survival in the neonatal hippocampus after cerebral hypoxiaischemia. Mol Neurodegener 7:17. CrossRef Medline

Talos F, Abraham A, Vaseva AV, Holembowski L, Tsirka SE, Scheel A, Bode D, Dobbelstein M, Brück W, Moll UM (2010) p73 is an essential regulator of neural stem cell maintenance in embryonal and adult CNS neurogenesis. Cell Death Differ 17:1816–1829. CrossRef Medline

Teixeira CM, Pomedli SR, Maei HR, Kee N, Frankland PW (2006) Involvement of the anterior cingulate cortex in the expression of remote spatial memory. J Neurosci 26:7555–7564. CrossRef Medline

Tissir F, Ravni A, Achouri Y, Riethmacher D, Meyer G, Goffinet AM (2009) DeltaNp73 regulates neuronal survival in vivo. Proc Natl Acad Sci U S A 106:16871–16876. CrossRef Medline

Westfall MD, Mays DJ, Sniezek JC, Pietenpol JA (2003) The Delta Np63 alpha phosphoprotein binds the p21 and 14-3-3 sigma promoters in vivo and has transcriptional repressor activity that is reduced by Hay-Wells syndrome-derived mutations. Mol Cell Biol 23:2264–2276. CrossRef Medline

Wetzel MK, Naska S, Laliberté CL, Rymar VV, Fujitani M, Biernaskie JA, Cole CJ, Lerch JP, Spring S, Wang SH, Frankland PW, Henkelman RM, Josselyn SA,

Sadikot AF, Miller FD, Kaplan DR (2008) p73 regulates neurodegeneration and phospho-tau accumulation during aging and Alzheimer's disease. Neuron 59:708–721. CrossRef Medline

Yang A, McKeon F (2000) P63 and P73: P53 mimics, menaces and more. Nat Rev Mol Cell Biol 1:199–207. CrossRef Medline

Yiu AP, Rashid AJ, Josselyn SA (2011) Increasing CREB function in the CA1 region of dorsal hippocampus rescues the spatial memory deficits in a mouse model of Alzheimer's disease. Neuropsychopharmacology 36: 2169–2186. CrossRef Medline